Modeling the photochemical transformation of nitrobenzene under conditions relevant to sunlit surface waters: Reaction pathways and formation of intermediates

(Article begins on next page)

22 November 2024

Modeling the photochemical transformation of nitrobenzene under conditions relevant to sunlit surface waters: Reaction pathways and formation of intermediates

Davide VIONE[(1)]*, **Elisa DE LAURENTIIS**[(1)], **Silvia BERTO**[(1)], **Claudio MINERO**[(1)],
Arzu HATIPOGLU[(2)], **Zekiye CINAR**[(2)]

(1) Università degli Studi di Torino, Dipartimento di Chimica, Via P.Giuria 5, 10125

Torino, Italy

(2) Yildiz Technical University, Department of Chemistry, 34220 Istanbul, Turkey

---

ABSTRACT

Nitrobenzene (NB) would undergo photodegradation in sunlit surface waters, mainly by direct photolysis and triplet-sensitized oxidation, with a secondary role of the $^\bullet$OH reaction. Its photochemical half-life time would range from a few days to a couple of months under fair-weather summertime irradiation, depending on water chemistry and depth. NB phototransformation gives phenol and the three nitrophenol isomers, in different yields depending on the considered pathway. The minor $^\bullet$OH role in degradation would make NB unsuitable as $^\bullet$OH probe in irradiated natural water samples, but the selectivity towards $^\bullet$OH could be increased by monitoring the formation of phenol from NB+$^\bullet$OH. The relevant reaction would proceed through *ipso*-addition of $^\bullet$OH on the carbon atom bearing the nitro-group, forming a pre-reactive complex that would evolve into a transition state (and then into a radical addition intermediate) with very low activation energy barrier.

Corresponding author   Fax: +39-011-6705242   E-mail: davide.vione@unito.it

Phone: +39-011-6705296

1. INTRODUCTION

Nitrobenzene (NB) is a nitroaromatic compound used in several industrial applications, mostly as an intermediate in the synthesis of aniline to finally produce rubber chemicals, pesticides, azo dyes, explosives and pharmaceuticals (including paracetamol) (Bhatkhandea et al., 2003).

The nitro group makes NB fairly resistant to biological degradation. Because of incomplete removal by wastewater treatment plants (Chen et al., 2014; Xia et al., 2014), NB may occur in surface waters up to $\mu g \ L^{-1}$ levels (Jin et al., 1998; Kang et al., 2001; Wang et al., 2002; Wang et al., 2003; He et al., 2006; Gao et al., 2013). Among the natural attenuation processes, biodegradation is possible but predictably slow (Jin and Rolle, 2014; Liu et al., 2014). Alternatively, photodegradation may occur by both direct photolysis (absorption of sunlight by NB, triggering degradation) and indirect photochemistry. In the latter, sunlight is absorbed by photosensitizers (chromophoric dissolved organic matter - CDOM-, nitrate and nitrite) to produce reactive transients such as the hydroxyl ($^{\bullet}OH$) and carbonate ($CO_3^{-\bullet}$) radicals, singlet oxygen ($^1O_2$) and CDOM triplet states ($^3CDOM^*$) (Canonica, 2007; Richard et al., 2007; Fenner et al., 2013). In addition to reacting with pollutants, $^{\bullet}OH$ and $CO_3^{-\bullet}$ are mainly scavenged by DOM (either chromophoric or not),

2

$^1O_2$ is deactivated by collision with water, and $^3CDOM^*$ is scavenged by O_2 to yield $^1O_2$ (Vione et al., 2014). Photochemistry might be an important pathway for NB degradation (Vialaton and Richard, 2002), but very limited evidence is available concerning the NB lifetime in natural settings.

NB is also a satisfactory $^{\bullet}OH$ probe in simplified laboratory systems (Vione et al., 2009), while its use as probe in irradiated surface waters is problematic because of interference by photolysis and $^3CDOM^*$ reactions (Vialaton and Richard, 2002; Vione et al., 2010).

The present paper aims at: *(i)* assessing by modeling, for the first time to our knowledge, the photochemical NB lifetime in surface-water environments, as a function of water chemistry and depth; *(ii)* elucidating the mechanism of NB reaction with $^{\bullet}OH$, and *(iii)* assessing whether the selectivity of NB as $^{\bullet}OH$ probe may be improved by taking into account the formation of intermediates.

2. METHODS AND PROCEDURES

2.1. Irradiation Experiments

Samples to be irradiated (5 mL total volume) were introduced into cylindrical Pyrex glass cells (diameter 4.0 cm, height 2.5 cm), tightly closed with a screw cap on the side neck. The samples were magnetically stirred during irradiation. The direct photolysis of NB was studied under a Philips TL 01 UV-Vis lamp, with emission maximum at 313 nm. Hydrogen peroxide was used as $^{\bullet}OH$ source under UVA irradiation (lamp Philips TL K05, emission maximum at 365 nm), to limit the NB direct photolysis. The same UVA lamp was used to irradiate NB in the presence of anthraquinone-2-sulphonate (AQ2S). Emission

(lamp) and absorption spectra are reported in **Figure SM1** of the Supplementary Material (hereafter SM). After irradiation, the time evolution of NB, phenol and nitrophenols was monitored by liquid chromatography (see SM for further details).

2.2. Kinetic Data Treatment

The reported concentration *vs.* time data of NB and its transformation intermediates are the average results of triplicate runs. The NB time evolution data were fitted with equation (1):

$$C_t = C_o \exp(-k_{NB}^d t) \tag{1}$$

where C_t is NB concentration at the time t, C_o its initial concentration, and k^d_{NB} the pseudo-first order degradation rate constant. The initial NB transformation rate is $R_{NB} = k^d_{NB} C_o$. The time evolution of each transformation intermediate was fitted with equation (2):

$$C_{\text{int},t} = \frac{k_{\text{int}}^f C_o [\exp(-k_{NB}^d t) - \exp(-k_{\text{int}}^d t)]}{k_{\text{int}}^d - k_{NB}^d} \tag{2}$$

where C_o, k^d_{NB} and t are as above, $C_{\text{int},t}$ is the concentration of the intermediate at the time t, and k^f_{int}, k^d_{int} are its pseudo-first order formation and transformation rate constants, respectively. The initial formation rate of each intermediate is $R_{\text{int}} = k^f_{\text{int}} C_o$, which is also the slope of the tangent to the relevant time evolution curve ($C_{\text{int},t}$ *vs.* t) at $t \to 0$. The intermediate yields were derived as the ratio of their initial rates to that of NB, $\eta_{\text{int}} = R_{\text{int}} R_{NB}^{-1}$.

2.3. Photochemical Modeling

The NB phototransformation kinetics under conditions relevant to surface waters was modeled with the APEX software (Aqueous Photochemistry of Environmentally-occurring Xenobiotics). It predicts photochemical half-life times of pollutants, formation kinetics and

yields of intermediates as a function of water chemistry and depth, for compounds with known direct photolysis quantum yields and second-order reaction rate constants with transient species (Vione, 2014; Bodrato and Vione, 2014). APEX results have been validated by comparison with field data of phototransformation kinetics in surface freshwaters (Maddigapu et al., 2011; Vione et al., 2011; De Laurentiis et al., 2012; Marchetti et al., 2013). APEX applies to well-mixed water bodies, including the epilimnion of stratified lakes.

2.4. Computational Set-up and Methodology

Quantum mechanical modeling techniques were employed to determine the reaction mechanism of NB+$^\bullet$OH. The relevant calculations were carried out with the DFT method, within the GAUSSIAN 03 package (Frisch et al., 2003). The DFT calculations used the hybrid B3LYP functional, which combines Hartree-Fock and Becke exchange terms with the Lee-Yang-Parr correlation functional. Concerning the choice of the basis set, optimizations were performed at the B3LYP/6-31G(d) level followed by single-point energy calculations at the B3LYP/6-311+G(d,p) level (Wong and Radom, 1998; Ozen et al., 2003). Zero-point vibrational energies (ZPEs) were calculated at the B3LYP/6-31G(d) level, and the same ZPEs were used for B3LYP/6-311+G(d,p)// B3LYP/6-31G(d) calculations.

The solvent effect on the reaction was taken into account with the COSMO solvation model, which describes the solvent reaction field by means of apparent polarization charges distributed on the cavity surface (Barone and Cossi, 1998; Hush et al., 2005).

3. RESULTS AND DISCUSSION

3.1. Photochemical Reactions of NB

The second-order reaction rate constant between NB and $^{\bullet}OH$ is reported in the literature ($k_{NB,^{\bullet}OH} = 3.9 \cdot 10^9$ M^{-1} s^{-1}; Buxton et al., 1988). No data are available for the NB reactivity with $^1O_2$, but electron-poor aromatics have $^1O_2$ reaction rate constants around 10^3 M^{-1} s^{-1} (Wilkinson and Brummer, 1981). Reaction between electron-poor NB and $^1O_2$ should thus be unimportant in surface waters, and Vialaton and Richard (2002) have excluded it upon irradiation of surface water samples or humic acids. NB would also be unreactive with $CO_3^{-\bullet}$ (Vione et al., 2009). Among the remaining photoreactions of environmental significance, direct photolysis and reaction with $^3CDOM^*$ were assessed here.

We used AQ2S as CDOM proxy to measure the reaction rate constant between NB and AQ2S triplet state ($^3AQ2S^*$). The AQ2S proxy has some experimental advantages: it has very-well known photophysics and photochemistry (which allows the second-order rate constants with $^3AQ2S^*$ to be easily measured upon steady irradiation) (Maddigapu et al., 2010), and it does not produce $^1O_2$ or $^{\bullet}OH$. The latter would be confounding factors in NB reactivity assessment (especially $^{\bullet}OH$), also because the use of scavengers (unnecessary with AQ2S) causes considerable problems related to their sometimes poor selectivity (Maddigapu et al., 2010).

The experiments carried out to study NB direct photolysis and reaction with $^3AQ2S^*$ are described in the SM. The results (direct photolysis quantum yield and reaction rate constant with $^3AQ2S^*$) are reported in **Table 1**.

3.2 Transformation Intermediates

The formation yields of phenol and nitrophenols from NB were assessed in the main NB photochemical processes in surface waters, namely direct photolysis and reactions with $^\bullet$OH and ^{3}CDOM*. The results of the irradiation experiments, carried out using ~0.1 mM NB to facilitate the quantification of the intermediates, are reported in **Figure SM3(SM)** for direct photolysis (**SM3a**), irradiation with H_2O_2 (**SM3b**), and irradiation with AQ2S (**SM3c**). The yields of the monitored intermediates (phenol, 2NP, 3NP and 4NP) are reported in **Table 1**.

The reaction with $^\bullet$OH (H_2O_2 irradiation) yielded the four intermediates (2NP > phenol > 3NP > 4NP) with almost quantitative conversion. Within experimental error, the mass balance of transformed NB was fully accounted for by phenol and nitrophenols. The yields under direct photolysis (2NP > 3NP > 4NP > phenol) were considerably lower compared to $^\bullet$OH, especially for phenol (η_{Phenol,H_2O_2} ~20 $\eta_{Phenol,Phot}$, see **Table 1**). With irradiated AQ2S only the nitrophenols were detected (2NP > 3NP > 4NP), while phenol was below the detection limit. Nitrophenols closed the mass balance of transformed NB under AQ2S irradiation, thereby excluding important formation of phenol followed by its fast degradation.

3.3 Computational Modeling of the Reactions with $^\bullet$OH

The $^\bullet$OH reactions with aromatic compounds proceed mainly by three mechanisms: H-atom abstraction from either *(i)* the side-chains or *(ii)* the ring(s), and *(iii)* aromatic ring addition (Kilic et al., 2007). Four different paths for the reaction of NB with $^\bullet$OH were determined, excluding ring abstraction paths that are negligible at room temperature due to large energy barriers (Brezova et al., 1995; Kilic et al., 2007). The four reaction paths,

ortho-addition (*o*-add), *meta*-addition (*m*-add), *para*-addition (*p*-add) and *ipso*-addition (*i*-add), are shown below:

$$(o\text{-R}) \qquad (3)$$

$$(m\text{-R}) \qquad (4)$$

$$(p\text{-R}) \qquad (5)$$

$$(i\text{-R}) \qquad (6)$$
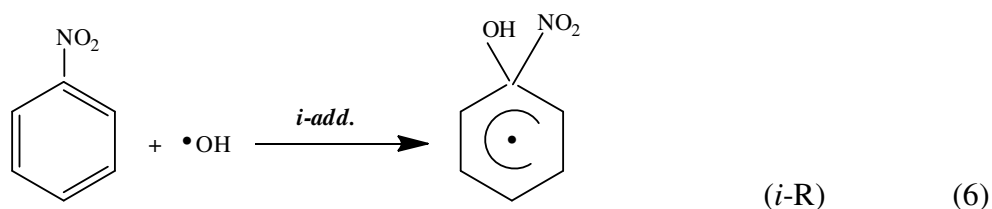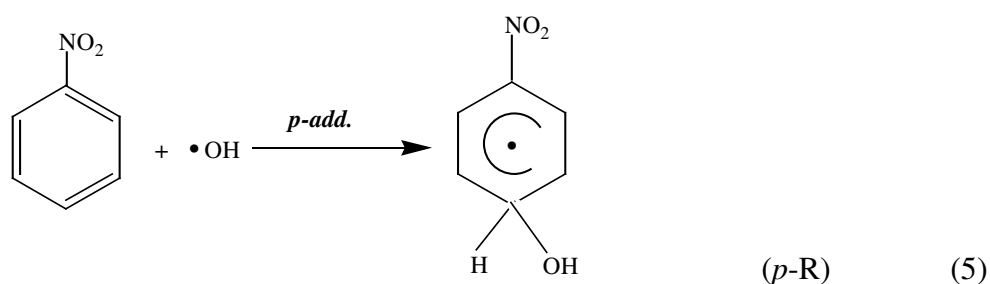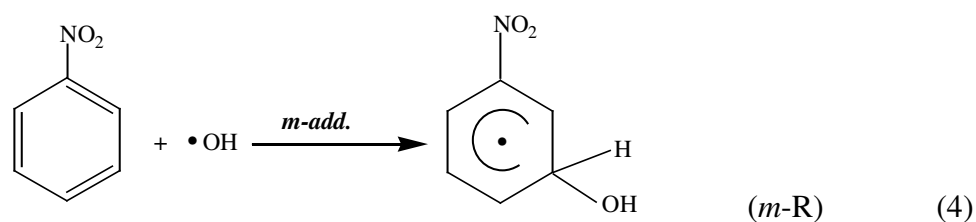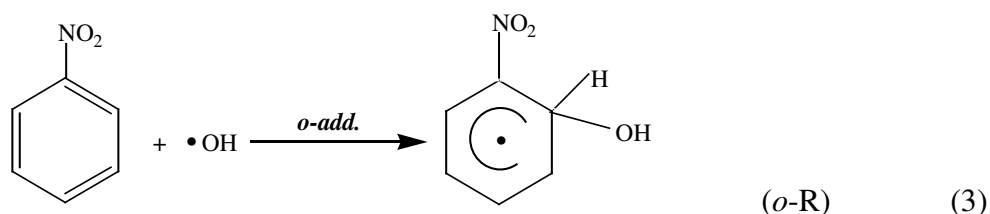
The $^\bullet$OH radical attacks a ring carbon with its unpaired electron and upon contact forms a C-O bond, while a π-bond of the aromatic system is broken and a hydroxynitrocyclohexadienyl radical (*o*-R, *m*-R, *p*-R or *i*-R) is formed. The relevant radicals are the precursors of 2NP, 3NP, 4NP and phenol, respectively.

Figure 1 represents the potential energy profile of the DFT-modeled mechanism for the initial attack of the $^\bullet$OH radical to NB (**1a**: gas phase; **1b**: aqueous solution). Our calculations indicated the formation of weakly bound van der Waals complexes (pre-

reactive complexes, PCs) between $^\bullet$OH and NB (see **Figure SM4(SM)** for the PCs optimized structures). The $^\bullet$OH radical is seen to approach the aromatic ring from above, lying almost parallel to the ring plane. The PCs cause the reaction paths under investigation to proceed over barriers that are lower in energy than the reactants. Furthermore, the presence of the complexes affects the reaction dynamics by spatially directing the reaction site, either by steric direction or by providing a potential well that favors a reaction site. Energetically, the PCs stability (from the most to the least stable) in aqueous solution is as follows: *m*-PC > *o*-PC > *p*-PC > *i*-PC. Interestingly, PCs would be more stable in the aqueous than in the gas phase because of the occurrence of hydrogen bonds with water molecules.

Four transition state complexes TS were identified (*o*-TS, *m*-TS, *p*-TS and *i*-TS), one for each of the possible reaction paths (see **Figure SM5(SM)** for their optimized structures). In all the complexes, the $^\bullet$OH radical is oriented such that it is almost parallel to the ring plane. In the light of the potential energy profiles reported in **Figure 1**, it may be suggested that the length of the forming C-O bond is a sensitive measure of the formation of the TS complex along the reaction coordinate. The C-O bonds of *p*-TS and *i*-TS (2.511 and 2.622 Å, respectively) are much longer than those of *m*-TS and *o*-TS, which suggests that *p*-TS and *i*-TS are early transition states. In contrast, *m*-TS and *o*-TS would be formed later along the reaction coordinate. All the TS energies are below those of the reactants, and their stability (from the most to the least stable) is *p*-TS > *i*-TS > *o*-TS > *m*-TS. In the aqueous phase the energies of all the TSs are decreased by around 15 kcal mol^{-1} compared to the gas phase, but *p*-TS and *i*-TS are still the most thermodynamically stable ones.

The radical species R, determined as the intermediate products of the reaction between NB and $^\bullet$OH, show the following stability order (from the most to the least stable): *p*-R >

o-R > *i*-R > *m*-R, both in the gas and in the aqueous phase. They are further stabilized in the aqueous phase, due to formation of hydrogen bonds with the solvent. The hydrogen bonds, either inter-molecular (aqueous solution) or intra-molecular (gas phase), account for the higher stability of the investigated radicals compared to the reactants (NB+$^{\bullet}$OH). The reactions will thus proceed to the corresponding products, once the reactants are sufficiently close to each other.

The activation energies (E_a) of the different addition paths (see **Table SM1(SM)**) are in the order E_a(para) < E_a(ipso) < E_a(meta) < E_a(ortho) in the gas phase, and E_a(para) < E_a(ipso) < E_a(ortho) < E_a(meta) in the aqueous phase. Depending on the interplay between the breaking of intra-molecular hydrogen bonds and the formation of new inter-molecular ones, the water solvent increases E_a(para) and E_a(ipso), and decreases E_a(ortho) and E_a(meta). The overall effect is a partial leveling of the activation energies in the aqueous solution, compared to the gas phase.

The rate constant *k* for each reaction path was calculated by using the Transition State Theory for 300 K. The *k* in the Transition State Theory is given by Eq. (7):

$$k = \frac{k_B T}{h} \frac{q_{TS}}{q_T . q_{OH}} e^{-Ea/RT} \qquad (7)$$

where k_B is Boltzmann's constant, *T* is temperature, *h* is Planck's constant, *q*'s are molecular partition functions for TS and reactants (NB+$^{\bullet}$OH), and E_a is the activation energy. Each *q* function was assumed to be the product of the translational, rotational, vibrational and electronic partition functions of the corresponding species (Hehre et al., 1986).

The rate constant calculation results (**Table SM1(SM)**) indicate that, in the gas phase, k(ipso) > k(para) > k(meta) > k(ortho) while, in aqueous solution, k(ipso) > k(para) > k(ortho) > k(meta). In water, the main primary intermediate formed in the oxidative degradation of NB would thus be *i*-R (precursor of phenol), followed in order of decreasing importance by *p*-R (precursor of 4NP), *o*-R (2NP) and *m*-R (3NP). Experimental data of H_2O_2 irradiation show that 2NP was formed in higher amount compared to phenol, and 3NP compared to 4NP. However, because it is almost impossible to excite H_2O_2 without exciting NB at the same time, the NB direct photolysis might not be negligible with irradiated H_2O_2. Upon NB photolysis, the yield of 2NP is much higher than that of phenol, and the 3NP yield is higher than that of 4NP. Therefore, one can hypothesize that the observed intermediate yields with irradiated H_2O_2 could derive from the contributions of both $^{\bullet}OH$ reaction and photolysis.

3.4. Photochemical Modeling

The photochemical half-life time of NB was predicted with the APEX software, taking into account its absorption spectrum, direct photolysis quantum yield and reaction rate constants with $^{\bullet}OH$ and $^{3}CDOM^*$ (the latter with $^{3}AQ2S^*$ as proxy). The formation of intermediates was calculated by using the yields η_{int} reported in **Table 1**. The NB half-life time ($t_{1/2}^{NB}$) in surface waters during summertime would vary from a few days to over two months, and it would increase with depth and DOC (Dissolved Organic Carbon, see **Figure SM6(SM)**). Unimportant variations of $t_{1/2}^{NB}$ would take place with variable nitrate and nitrite, because of the limited role of $^{\bullet}OH$ in NB transformation in surface waters (*vide infra*). For the same reason, $t_{1/2}^{NB}$ would be poorly influenced by carbonate and bicarbonate. This result is consistent with Vialaton and Richard (2002), who report a secondary role of

$^\bullet$OH in NB degradation in irradiated natural water. The $t_{1/2}^{NB}$ would increase with depth, because the bottom layer of a deep water body is poorly illuminated by sunlight and would compensate for the elevated photoactivity at the water surface. The increase of $t_{1/2}^{NB}$ with DOC depends on the competition for irradiance between NB and CDOM, which would be more important in high-DOC waters (Vione et al., 2014) and would inhibit the direct photolysis.

Figure 2 reports the fractions of NB transformation accounted for by direct photolysis and reactions with $^\bullet$OH and ^{3}CDOM*, as a function of the formation quantum yield of ^{3}CDOM* from irradiated CDOM ($\Phi_{^3CDOM*}$). The quantity $\Phi_{^3CDOM*}$ may vary in different water bodies, and the reported 10^{-3}-$2 \cdot 10^{-2}$ range would encompass a reasonable variety of water environments (Vione et al., 2014). Higher values of $\Phi_{^3CDOM*}$ have been observed, but they are linked to extreme environments (lakes in the Antarctica) that showed a remarkably high photoactivity (De Laurentiis et al., 2013).

Figure 2a models the case of a shallow water body (1 m depth) with DOC = 1 mg C L^{-1}. The main processes of NB transformation would be direct photolysis (~90% of the total) and reaction with $^\bullet$OH (~10%), while the ^{3}CDOM* reaction would be unimportant for all the $\Phi_{^3CDOM*}$ values. The case of **Figure 2b** is quite different (10 m depth and DOC = 10 mg C L^{-1}). Such conditions are much more favorable to the ^{3}CDOM* process, which would account for 10-55% of NB transformation depending on $\Phi_{^3CDOM*}$, while the $^\bullet$OH reaction would be minor to negligible.

Vialaton and Richard (2002), in addition to a limited role of $^\bullet$OH, reported an important role of ^{3}CDOM* in NB transformation. Because they used irradiated humic substances as triplet sensitizers (which are usually characterized by elevated $\Phi_{^3CDOM*}$

values) at significant concentration (10 mg L^{-1}), there appears to be a good agreement between their experimental data and our modeling results.

Figure 2c reports the formation yields of phenol and nitrophenols from NB in the conditions of **Figure 2b**. Because the ^{3}CDOM* process yields nitrophenols but it does not yield phenol, by increasing $\Phi_{^3CDOM*}$ the yields of nitrophenols increase and that of phenol decreases.

The important transformation by photolysis and ^{3}CDOM* reaction would limit the use of NB to probe $^\bullet$OH in irradiated water samples. However, alternatively to substrate degradation, one may use the formation of intermediates to probe $^\bullet$OH. The potential validity of this approach was assessed by photochemical modeling, and **Figure 3** shows correlation plots between the APEX-modeled steady-state [$^\bullet$OH] (referred to 22 W m^{-2} UV irradiance) and the (pseudo-first order) formation/transformation rate constants predicted by APEX for NB, phenol and nitrophenols. Variable [$^\bullet$OH] was obtained by APEX modeling by assuming variable water conditions (nitrate, nitrite, DOC and depth). The best correlation ($r^2 = 0.97$) is observed between [$^\bullet$OH] and the rate constant of phenol formation (**Figure 3b**), but statistically significant correlation ($p < 0.01$) could also be found with the rate constants of NB degradation and nitrophenol formation. However, a correlation does not necessarily imply a mechanistic link: [$^\bullet$OH] would be high when the DOC is low, under which conditions the direct photolysis of NB would be enhanced by the limited absorption of sunlight by CDOM.

The formation rate of phenol from NB+$^\bullet$OH is given by $R_{Phenol} = \eta_{Phenol,^\bullet OH} \, k_{NB,^\bullet OH} \, [^\bullet OH] \, [NB]$, and the pseudo-first order reaction rate constant is $k_{Phenol} = R_{Phenol} \, [NB]^{-1} = \eta_{Phenol,^\bullet OH} \, k_{NB,^\bullet OH} \, [^\bullet OH]$, where $\eta_{Phenol,^\bullet OH}$ is reported in **Table 1** and $k_{NB,^\bullet OH} = 3.9 \cdot 10^9$ M^{-1} s^{-1} = $1.4 \cdot 10^{14}$ M^{-1} SSD^{-1} (1 SSD = $3.6 \cdot 10^4$ s under 22 W m^{-2}

UV irradiance; Bodrato and Vione, 2014). If phenol formation were accounted for by NB+$^\bullet$OH alone, the regression line to the plot of **Figure 3b** had a slope $\eta_{Phenol,^\bullet OH}\, k_{NB,^\bullet OH}$ = $3.9 \cdot 10^{13}$ M^{-1} SSD^{-1}. The actual slope is $(4.8\pm0.4)\cdot 10^{13}$ M^{-1} SSD^{-1}, implying that by considering phenol formation one would overestimate [$^\bullet$OH] by about 25%. This level of uncertainty is still acceptable in surface-water photochemistry. In contrast, by considering NB degradation ($k_{NB} = k_{NB,^\bullet OH}[^\bullet OH]$) or nitrophenol (NP) formation ($k_{NP} = (\eta_{2NP,^\bullet OH} + \eta_{3NP,^\bullet OH} + \eta_{4NP,^\bullet OH}) k_{NB,^\bullet OH}[^\bullet OH]$) and by making similar calculations as for phenol, one expects an overestimation of [$^\bullet$OH] by, respectively, five- and two-folds.

Finally, in section 3.3 it was speculated that the experimental data obtained under H_2O_2 irradiation might underestimate the $^\bullet$OH yield of phenol from NB. If the actual yield were higher than assumed here, the validity of the NB$\rightarrow$phenol transformation as $^\bullet$OH probe would be increased.

4. CONCLUSIONS

NB would be significantly photodegraded in surface waters, with half-life time ranging from few days to a couple of months in fair-weather summertime. NB phototransformation would proceed mainly by direct photolysis and triplet-sensitized oxidation, with a secondary role of the $^\bullet$OH reaction. This issue would make NB degradation unsuitable as $^\bullet$OH probe in irradiated natural water samples, but the $^\bullet$OH selectivity might be improved by monitoring the formation of phenol from NB. The reaction between NB and $^\bullet$OH gives phenol and the three nitrophenols as main intermediates. It proceeds first through weakly

bound van der Waals complexes (pre-reactive complexes) that then evolve into the transition states with very low activation energy barriers.

REFERENCES

Albinet, A., Minero, C., Vione, D., 2010. UVA irradiation induces direct phototransformation of 2,4-dinitrophenol in surface water samples. Chemosphere 80, 759-763.

Barone V., Cossi M., 1998. Quantum calculation of molecular energies and energy gradients in solution by a conductor solvent model. J. Phys. Chem. A. 102, 1995-2001.

Bhatkhandea, D.S., Pangarkara, V.G., Beenackers, A.A.C.M., 2003. Photocatalytic degradation of nitrobenzene using titanium dioxide and concentrated solar radiation: chemical effects and scaleup. Water Res. 37, 1223-1230.

Bodrato, M., Vione, D., 2014. APEX (Aqueous Photochemistry of Environmentally occurring Xenobiotics): A free software tool to predict the kinetics of photochemical processes in surface waters. Environ. Sci.: Processes Impacts 16, 732-740.

Brezova, V., Ceppan, M., Brandsteterova, E., Breza, M., Lapcik L., 1991. Photocatalytic hydroxylation of benzoic acid in aqueous titanium dioxide suspension. J. Photochem. Photobiol. A: Chem. 59, 385-391.

Buxton, G.V., Greenstock, C.L., Helman, W.P., Ross, A.B., 1988. Critical review of rate constants for reactions of hydrated electrons, hydrogen atoms and hydroxyl radicals ($^{\bullet}OH/^{\bullet}O^-$) in aqueous solution. J. Phys. Chem. Ref. Data 17, 1027-1284.

Canonica, S., Hellrung, B., Muller, P., Wirz, J., 2006. Aqueous oxidation of phenylurea herbicides by triplet aromatic ketones. Environ. Sci. Technol. 2006, 40, 6636-6641.

Canonica, S., 2007. Oxidation of aquatic organic contaminants induced by excited triplet states. Chimia 61, 641-644.

Chen, Y., Li, H. Y., Liu, W.J., Tu, Y., Zhang, Y.H., Han, W.Q., Wang, L.J., 2014. Electrochemical degradation of nitrobenzene by anodic oxidation on the constructed TiO_2-NTs/SnO_2-Sb/PbO_2 electrode. Chemosphere 113, 48-55.

Cory, R.M., McKnight, D.M., 2005. Fluorescence spectroscopy results reveals ubiquitous presence of oxidized and reduced quinones in dissolved organic matter. Environ. Sci. Technol. 39, 8142-8149.

De Laurentiis, E., Chiron, S., Kouras-Hadef, S., Richard, C., Minella, M., Maurino, V., Minero, C., Vione, D., 2012. Photochemical fate of carbamazepine in surface freshwaters: Laboratory measures and modeling. Environ. Sci. Technol. 46, 8164-8173.

De Laurentiis, E., Buoso, S., Maurino, V., Minero, C., Vione, D., 2013. Optical and photochemical characterization of chromophoric dissolved organic matter from lakes in Terra Nova Bay, Antarctica. Evidence of considerable photoreactivity in an extreme environment. Environ. Sci. Technol. 47, 14089-14098.

Fenner, K., Canonica, S., Wackett, L.P., Elsner, M., 2013. Evaluating pesticide degradation in the environment: Blind spots and emerging opportunities. Science 341, 752-758.

Frisch, M.J. , Trucks, G.W., Schlegel, H.B., Scuseria, G.E., Robb M.A., Cheeseman J.R., Montgomery Jr., J.A., Vreven, T., Kudin, K.N., Burant, J.C., Millam, J.M., Iyengar, S.S., Tomasi, J., Barone, V., Mennucci, B., Cossi, M., Scalmani, G., Rega, N., Petersson, G.A., Nakatsuji, H., Hada, M., Ehara, M., Toyota, K., Fukuda, R., Hasegawa, J., Ishida, M., Nakajima, T., Honda, Y., Kitao, O., Nakai, H., Klene, M., Li, X., Knox, J.E., Hratchian, H.P., Cross, J.B., Adamo, C., Jaramillo, J., Gomperts, R., Stratmann, R.E., Yazyev, O., Austin, A.J., Cammi, R., Pomelli, C., Ochterski, J.W., Ayala, P.Y., Morokuma, K., Voth, G.A., Salvador, P., Dannenberg, J.J., Zakrzewski, V.G., Dapprich, S., Daniels, A.D., Strain, M.C., Farkas, O., Malick, D.K., Rabuck, A.D., Raghavachari, K., Foresman, J.B., Ortiz, J.V., Cui, Q., Baboul, A.G., Clifford, S., Cioslowski, J., Stefanov, B.B., Liu, G., Liashenko, A., Piskorz, P., Komaromi, I., Martin, R.L., Fox, D.J., Keith, T., Al-Laham, M.A., Peng, C.Y., Nanayakkara, A., Challacombe, M., Gill, P.M.W., Johnson, B., Chen, W., Wong, M.W., Gonzalez, C., Pople, J.A., 2003. Gaussian 03, Revision B.04, Gaussian, Inc., Pittsburgh, PA.

Gao, J.J., Liu, X.R., Hao, H., Yuan, H., Zhou, H.D., 2013. Survey on typical organic pollutants and health risks of main water sources in Yellow River basin. Environ. Engineer. Manag. J. 12, 1751-1755.

He, M.C., Sun, Y., Li, X.R., Yang, Z.F., 2006. Distribution patterns of nitrobenzenes and polychlorinated biphenyls in water, suspended particulate matter and sediment from mid- and down-stream of the Yellow River (China). Chemosphere 65, 365-374.

Hehre, W.J., Radom, L., Schleyer, P.R., Pople, J.A., 1986. Ab initio Molecular Orbital Theory, Wiley, New York.

Hush, N.S., Schamberger, J., Bacskay, G.B., 2005. A quantum chemical computational study of the relative stabilities of cis- and transplatinum dichloride in aqueous solution. Coord. Chem. Rev. 249, 299-311.

Jin, Z., Li, S.R., Li, Q.S., 1998. Qualitative and quantitative analysis of organic constituents in Song Hua River's water by GC/MS. J. Chin. Mass Spectrom. Soc. 19, 33–42.

Jin, B., Rolle M., 2014. Mechanistic approach to multi-element isotope modeling of organic contaminant degradation. Chemosphere 95, 131-139.

Kang, Y.H., Gong, Z.Y., Wang, Z.J., Li, G.G., 2001. The study of VOCs in Guanting reservoir and Yongdinghe River. Acta Sci. Circum. 21, 338-342.

Kiliç, M., Kocturk, G., San, N., Cinar, Z., 2007. A model for product distributions for the reactions of phenol derivatives with hydroxyl radicals. Chemosphere 69, 1396-1408.

Liu, Z.Q., Cui, F.Y., Ma, H., Fan, Z.Q., Zhao, Z.W., Hou, Z.L., Liu, D.M., 2014. The transformation mechanism of nitrobenzene in the presence of a species of cyanobacteria Microcystis aeruginosa. Chemosphere 2014, 95, 234-240.

Maddigapu, P.R., Bedini, A., Minero, C., Maurino, V., Vione, D., Brigante, M., Mailhot, G., Sarakha, M., 2010. The pH-dependent photochemistry of anthraquinone-2-sulfonate. Photochem. Photobiol. Sci. 2010, 9, 323-330.

Maddigapu, P.R., Minella, M., Vione, D., Maurino, V., Minero, C., 2011. Modeling phototransformation reactions in surface water bodies: 2,4-Dichloro-6-nitrophenol as a case study. Environ. Sci. Technol. 45, 209-214.

Marchetti, G., Minella, M., Maurino, V., Minero, C., Vione, D., 2013. Photochemical transformation of atrazine and formation of photointermediates under conditions

relevant to sunlit surface waters: Laboratory measures and modelling. Wat. Res. 47, 6211-6222.

Ozen, A.S., Aviyente, V., Klein, R.A., 2003. Modeling the oxidative degradation of azo dyes: A density functional theory study. J. Phys. Chem. A. 107, 4898-4907.

Richard, C., Ter Halle, A., Sarakha, M., Mazellier, P., Chovelon, J. M., 2007. Solar light against pollutants. Actual. Chim. 308-309, 71-75.

Vialaton, D., Richard, C., 2002. Phototransformation of aromatic pollutants in solar light: Photolysis versus photosensitized reactions under natural water conditions. Aquat. Sci. 64, 207-215.

Vione, D., Khanra, S., Man, S.C., Maddigapu, P.R., Das, R., Arsene, C., Olariu, R.I., Maurino, V., Minero, C., 2009. Inhibition vs. enhancement of the nitrate-induced phototransformation of organic substrates by the $^\bullet$OH scavengers bicarbonate and carbonate. Water Res. 43, 4718-4728.

Vione, D., Ponzo, M., Bagnus, D., Maurino, V., Minero, C., Carlotti, M.E., 2010. Comparison of different probe molecules for the quantification of hydroxyl radicals in aqueous solution. Environ. Chem. Lett. 8, 95-100.

Vione, D., Maddigapu, P. R., De Laurentiis, E., Minella, M., Pazzi, M., Maurino, V., Minero, C., Kouras, S., Richard, C., 2011. Modelling the photochemical fate of ibuprofen in surface waters. Water Res. 45, 6725-6736.

Vione, D., 2014. A test of the potentialities of the APEX software (Aqueous Photochemistry of Environmentally-occurring Xenobiotics). Modelling the photochemical persistence of the herbicide cycloxydim in surface waters, based on literature kinetics data. Chemosphere 99, 272-275.

Vione, D., Minella, M., Maurino, V., Minero, C., 2014. Indirect photochemistry in sunlit surface waters: Photoinduced production of reactive transient species. Chem. Eur. J. 20, 10590-10606.

Wang, Z.J., Lv, Y.B., Wang, Y., Ma, M., 2002. Assessing the ecological risk of substituted benzenes in Huaihe River. China Acta Sci. Circum. 22, 300-304.

Wang, H., Yang, N.Y., Shen, Y.W., Wang, B., Wang, L.X., 2003. Safety assessment on several organic pollutants of the Haihe River valley. Res. Environ. Sci. 16, 35-36.

Wilkinson, F., Brummer, J., 1981. Rate constants for the decay and reactions of the lowest electronically excited singlet-state of molecular oxygen in solution. J. Phys. Chem. Ref. Data 10, 809-1000.

Wong M.W., Radom L., 1998. Radical additions to alkenes: Further assessment of theoretical procedures, J. Phys. Chem. A 102, 2237-2245.

Xia, K., Xie, F., Ma, Y., 2014. Degradation of nitrobenzene in aqueous solution by dual-pulse ultrasound enhanced electrochemical process. Ultrason. Sonochem. 21, 549-553.

Table 1. Direct photolysis quantum yield and second-order reaction rate constants of NB with $^\bullet$OH and ^{3}AQ2S*. Formation yields of phenol and

nitrophenols from NB, upon direct photolysis and reactions with $^\bullet$OH and ^{3}AQ2S* (calculated as the ratio between the formation rates

of intermediates and the degradation rate of NB). The error bounds represent $\pm\sigma$. In the case of the yields, they were calculated by

means of the rules of error propagation.

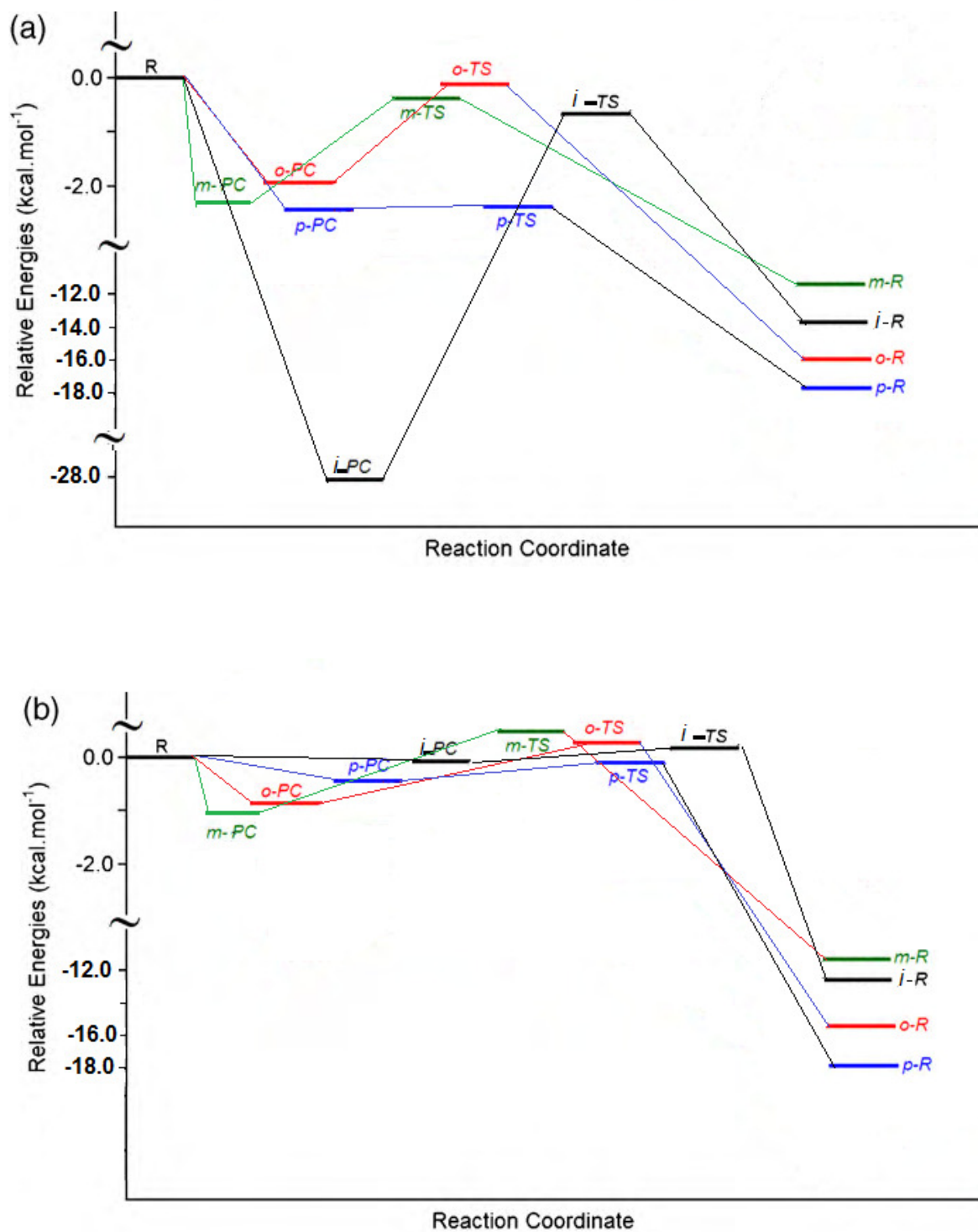|	*Direct photolysis*	*$^\bullet$OH*	*^{3}AQ2S**
Nitrobenzene (NB)	$\Phi_{NB} = (5.7\pm1.1)\cdot10^{-3}$	$k_{NB,^\bullet OH} = 3.9\cdot10^{9}\ \mathrm{M^{-1}\ s^{-1}}$ (a)	$k_{NB,^3AQ2S*} = (1.1\pm0.1)\cdot10^{8}\ \mathrm{M^{-1}\ s^{-1}}$
Phenol	$\eta_{Phenol,Phot} = (1.4\pm0.3)\cdot10^{-2}$	$\eta_{Phenol,^\bullet OH} = 0.28\pm0.14$	$\eta_{Phenol,^3AQ2S*} = -$
2-Nitrophenol (2NP)	$\eta_{2NP,Phot} = (7.5\pm1.7)\cdot10^{-2}$	$\eta_{2NP,^\bullet OH} = 0.35\pm0.14$	$\eta_{2NP,^3AQ2S*} = 0.54\pm0.16$
3-Nitrophenol (3NP)	$\eta_{3NP,Phot} = (5.3\pm1.0)\cdot10^{-2}$	$\eta_{3NP,^\bullet OH} = 0.17\pm0.09$	$\eta_{3NP,^3AQ2S*} = 0.25\pm0.05$
4-Nitrophenol (4NP)	$\eta_{4NP,Phot} = (2.2\pm0.4)\cdot10^{-2}$	$\eta_{4NP,^\bullet OH} = 0.12\pm0.05$	$\eta_{4NP,^3AQ2S*} = 0.16\pm0.05$

(a) Buxton et al., 1988.

Figure 1. The potential energy profile of the DFT-modeled mechanism for the reaction of NB+ •OH in **(a)** gas phase and **(b)** aqueous media.
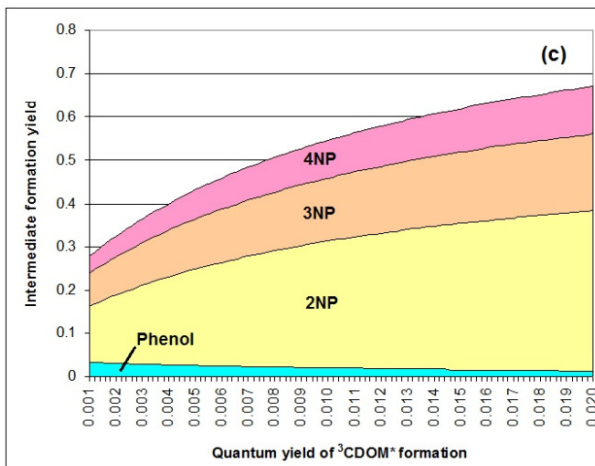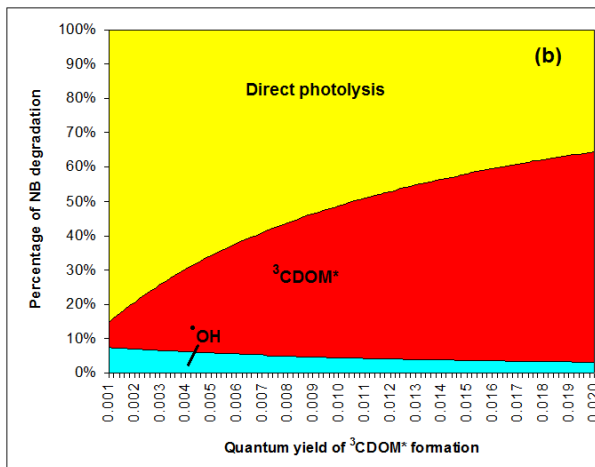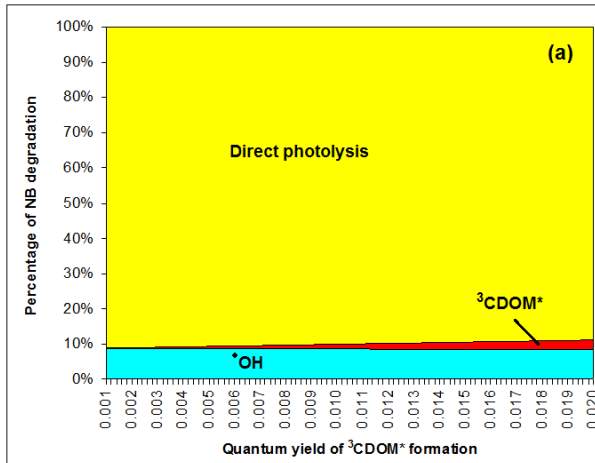
Figure 2. Modelled fraction of NB transformation accounted for by direct photolysis and reaction with $^\bullet OH$ and $^3CDOM^*$, as a function of $\Phi_{^3CDOM^*}$. **(a)** d = 1 m, DOC = 1 mg C L^{-1}; **(b)** d = 10 m, DOC = 10 mg C L^{-1}. Other water conditions: 0.1 mM NO_3^-, 1 µM NO_2^-, 1 mM HCO_3^-, 10 µM CO_3^{2-}. **(c)** Modelled yields of phenol and nitrophenols from NB, as a function of $\Phi_{^3CDOM^*}$. Water conditions are the same as for case (b).
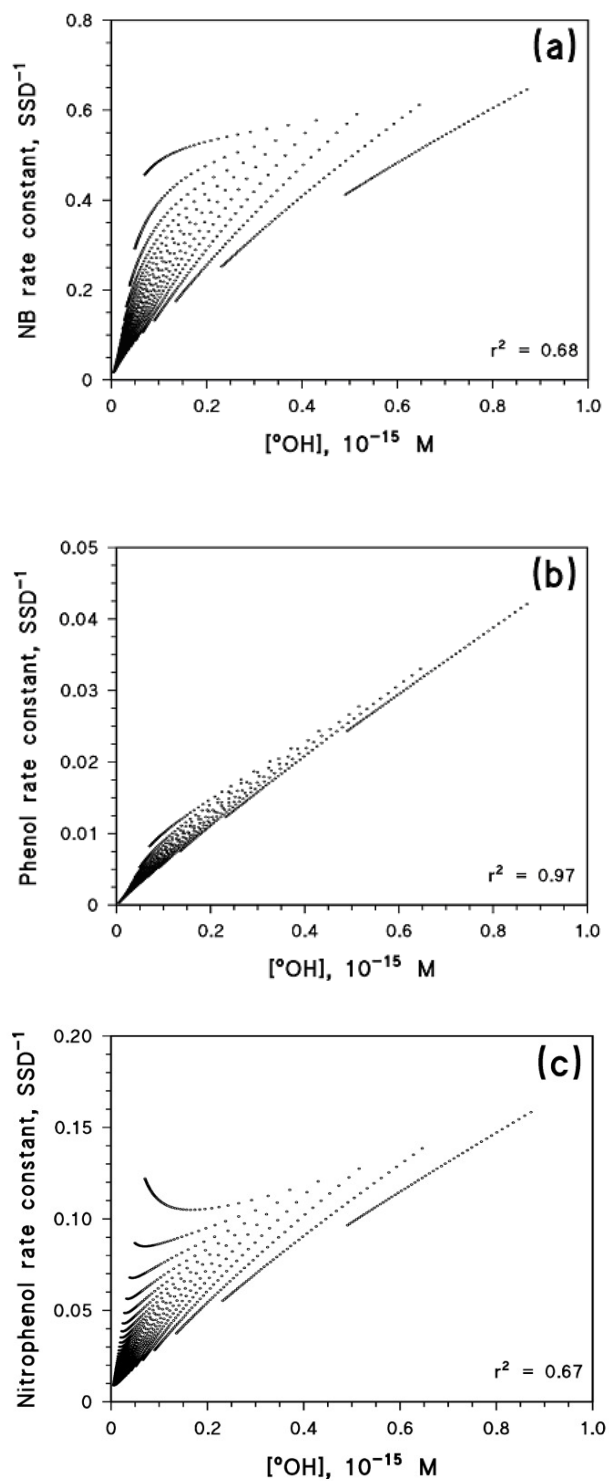
Figure 3. Correlation plot between modelled [$^{\bullet}$OH] (steady-state concentration under 22 W m^{-2} UV irradiance of sunlight) and other modelled quantities: **(a)** NB degradation rate constant; **(b)** phenol formation rate constant; **(c)** nitrophenol formation rate constant. In photochemical modelling it was hypothesized $\Phi_{^3CDOM*} = 0.01$.

SUPPLEMENTARY MATERIAL

Modeling the photochemical transformation of nitrobenzene under conditions relevant to sunlit surface waters: Reaction pathways and formation of intermediates

Davide VIONE[(1)]*, **Elisa DE LAURENTIIS**[(1)], **Silvia BERTO**[(1)], **Claudio MINERO**[(1)], **Arzu HATIPOGLU**[(2)], **Zekiye CINAR**[(2)]

(2) Università degli Studi di Torino, Dipartimento di Chimica, Via P.Giuria 5, 10125 Torino, Italy

(2) Yildiz Technical University, Department of Chemistry, 34220 Istanbul, Turkey

_____

ABSTRACT

Nitrobenzene (NB) would undergo photodegradation in sunlit surface waters, mainly by direct photolysis and triplet-sensitized oxidation, with a secondary role of the $^\bullet$OH reaction. Its photochemical half-life time would range from a few days to a couple of months under fair-weather summertime irradiation, depending on water chemistry and depth. NB phototransformation gives phenol and the three nitrophenol isomers, in different yields depending on the considered pathway. The minor $^\bullet$OH role in degradation would make NB unsuitable as $^\bullet$OH probe in irradiated natural water samples, but the selectivity towards $^\bullet$OH could be increased by monitoring the formation of phenol from NB+$^\bullet$OH. The relevant reaction would proceed through *ipso*-addition of $^\bullet$OH on the carbon atom bearing the nitro-group, forming a pre-reactive complex that would evolve into a transition state (and then into a radical addition intermediate) with very low activation energy barrier.

Keywords: Nitrobenzene, hydroxyl radical, photo-oxidative degradation, DFT calculation, COSMO

_____

Corresponding author   Fax: +39-011-6705242   E-mail: davide.vione@unito.it
   Phone: +39-011-6705296

Reagents and materials

Nitrobenzene (NB, purity grade >99.5 %) was purchased from Fluka, H_2O_2 (35 %), H_3PO_4 (85 %), phenol (>99 %), 3- and 4-nitrophenol (99%) and anthraquinone-2-sulphonic acid, sodium salt (AQ2S, 97%) from Aldrich, 2-nitrophenol (>99 %) and acetonitrile (LiChrosolv gradient grade) from VWR Int. All reagents were used as received, without further purification.

Irradiation experiments

The photon flux reaching the irradiated solutions was determined by ferrioxalate actinometry.[1] The emission spectra of the lamps were measured with an Ocean Optics SD 2000 CCD spectrophotometer and normalized to the actinometry results, taking into account the transmittance of the Pyrex glass. The lamp spectra are reported in **Figure SM1**. The figure also reports the molar absorption coefficients of H_2O_2, NB and AQ2S, measured with a Varian Cary 100 Scan UV-Vis spectrophotometer.

After irradiation, the samples were analyzed by High Performance Liquid Chromatography coupled with UV detection. The adopted Merck-Hitachi instrument was equipped with AS2000A auto-sampler (100 µL sample volume), L-6200 and L-6000 pumps for high-pressure gradients, Merck LiChrocart RP-C18 column packed with LiChrospher 100 RP-18 (125 mm × 4.6 mm × 5 µm), and L-4200 UV-Vis detector (detection wavelength 210 nm). It was adopted an isocratic elution with a 40:60 mixture of acetonitrile:aqueous H_3PO_4 (pH 2.8), at a flow rate of 1.0 mL min^{-1}. The retention times (in minutes) were as follows: phenol 2.6, 4-nitrophenol (4NP) 3.0, 3-nitrophenol (3NP) 3.2, 2-nitrophenol (2NP) 5.9, nitrobenzene (NB) 6.4. The column dead time was 0.9 min.

---

[1] H. J. Kuhn, S. E. Braslavsky, R. Schmidt, Chemical actinometry. Pure Appl. Chem. (2004) 76, 2105-2146.
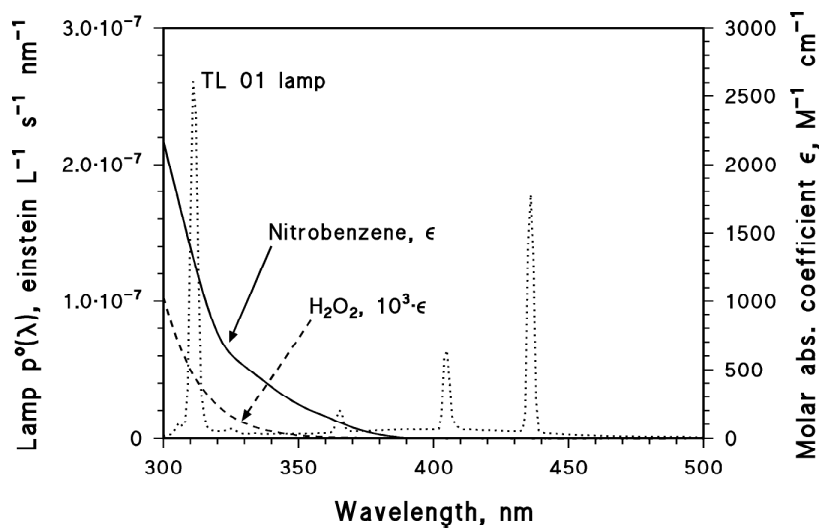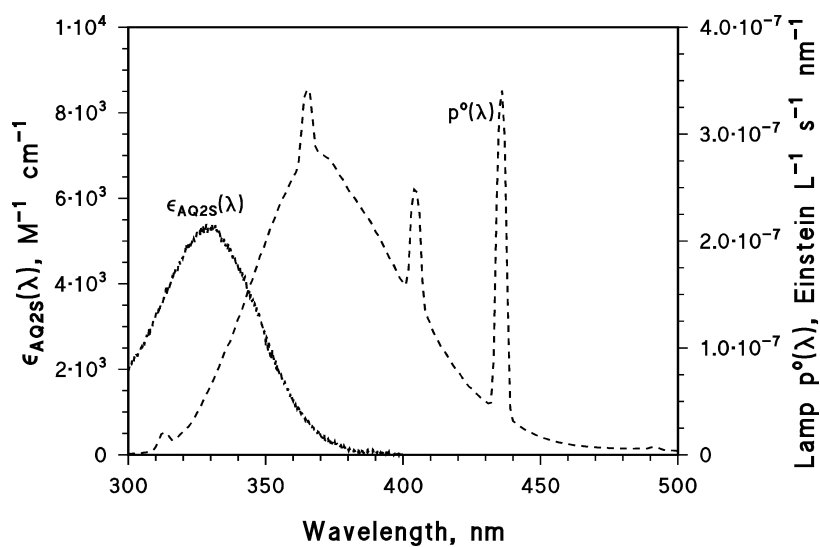
Figure SM1. **(a)** Absorption spectra of nitrobenzene (NB) and H_2O_2. Incident spectral photon flux density of the UVB lamp (Philips TL 01 20W).

(b) Absorption spectrum of antraquinone-2-sulphonate (AQ2S). Incident spectral photon flux density of the UVA lamp (Philips TL K05 40W).

Direct photolysis

NB (initial concentration 0.1 mM) was irradiated under the TL 01 lamp (emission maximum at 313 nm, see **Figure SM1**) at pH 6 (natural pH). A control run was also carried out in the dark, by wrapping the cylindrical cells containing the solutions in double aluminium foil, and by placing them under the same lamp used for irradiation experiments. In this way, comparable temperature and stirring conditions as for the irradiation experiments would be achieved. The transformation of NB in the dark was negligible.

Under the adopted conditions, irradiated NB followed a pseudo-first order transformation kinetics with $R_{NB} = (2.61\pm0.53)\cdot10^{-9}$ M s^{-1} ($\mu\pm\sigma$). The photon flux absorbed by NB can be expressed as $P_a^{NB} = \int_\lambda p°(\lambda)\,[1-10^{-\varepsilon_{NB}(\lambda)b[NB]}]d\lambda = 4.6\cdot10^{-7}$ Einstein L^{-1} s^{-1}, where $p°(\lambda)$ is the incident spectral photon flux density of the UVB lamp, $\varepsilon_{NB}(\lambda)$ the molar absorption coefficient of NB (see **Figure SM1**), $b = 0.4$ cm the optical path length in solution and [NB] = 0.1 mM. From these data it is possible to obtain the polychromatic photolysis quantum yield of NB between 300 and 400 nm, where the spectra of the lamp and NB overlap, as $\Phi_{NB} = R_{NB}\,(P_a^{NB})^{-1} = (5.7\pm1.1)\cdot10^{-3}$.

Reaction with irradiated AQ2S

Figure SM2 reports the initial transformation rate of NB (R_{NB}) as a function of its initial concentration, upon UVA irradiation of 0.1 mM AQ2S at pH 6. The direct photolysis of NB (irradiation without AQ2S) was negligible at the adopted irradiation time scale (up to 8 h).
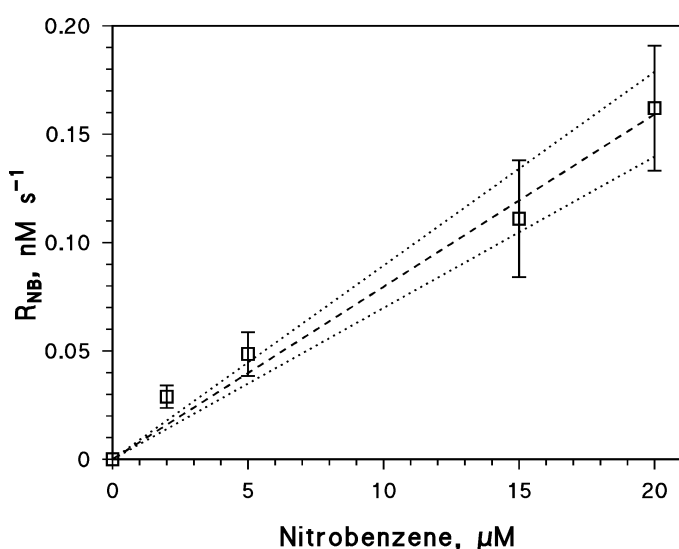

Figure SM2. Initial transformation rates of nitrobenzene (NB) upon UVA irradiation of 0.1 mM AQ2S, as a function of the initial NB concentration. The solution pH was 6. The fit line is dashed, the dotted ones represent the 95% confidence limits of the fit. The error bounds to the rate data represent $\pm\sigma$.

The triplet state ^{3}AQ2S*, which is the main reactive species of AQ2S under irradiation, has a formation quantum yield $\Phi_{^3AQ2S*} = 0.18$ and a first-order deactivation rate constant $k_{^3AQ2S*} = 5.0 \cdot 10^6$ s^{-1}.[2,3,4] The formation rate of ^{3}AQ2S* would be $R_{^3AQ2S*} = \Phi_{^3AQ2S*} \; P_a^{AQ2S}$ (where P_a^{AQ2S} is the photon flux absorbed by AQ2S, in units of Einstein L^{-1} s^{-1}). The transformation or deactivation of ^{3}AQ2S* would be in competition with the reaction with the substrate S (rate constant $k_{^3AQ2S*,S}$, see Scheme below, with ISC = inter-system crossing).[4,5] Reaction between ^{3}AQ2S* and ground-state AQ2S can be minimised by adopting an AQ2S initial concentration of 0.1 mM or lower.[6]
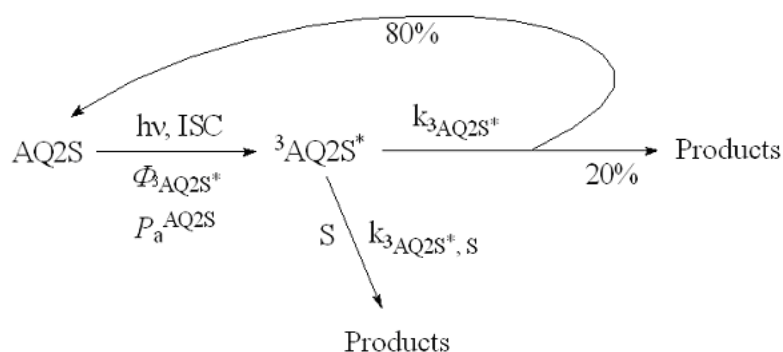
Upon application of the steady-state approximation to ^{3}AQ2S*, the transformation rate of S by irradiated AQ2S can be expressed as follows:

$$R_S = \Phi_{^3AQ2S*} \cdot P_a^{AQ2S} \cdot \frac{k_{^3AQ2S*,S} \cdot [S]}{k_{^3AQ2S*} + k_{^3AQ2S*,S} \cdot [S]} \qquad (S1)$$

Under the hypothesis that $k_{^3AQ2S*,S} \cdot [S] \ll k_{^3AQ2S*}$, one gets:

$$R_S = \Phi_{^3AQ2S*} \cdot P_a^{AQ2S} \cdot \frac{k_{^3AQ2S*,S}}{k_{^3AQ2S*}} \cdot [S] \qquad (S2)$$

In the present case, the molar absorption coefficient of S = NB at 365 nm (the wavelength of the lamp emission maximum) is five times lower than for AQ2S. When considering that the NB initial

[2] I. Loeff, A. Treinin, H. Linschitz, Photochemistry of 9,10-anthraquinone-2-sulfonate in solution. 1. Intermediates and mechanism, J. Phys. Chem. 87 (1983) 2536-2544.
[3] A.E. Alegría, A. Ferrer, G. Santiago, E. Sepúlveda, W. Flores, Photochemistry of water-soluble quinones. Production of the hydroxyl radical, singlet oxygen and the superoxide ion, J. Photochem. Photobiol. A: Chem. 127 (1999) 57-65.
[4] P.R. Maddigapu, A. Bedini, C. Minero, V. Maurino, D. Vione, M. Brigante, G. Mailhot, M. Sarakha, The pH-dependent photochemistry of anthraquinone-2-sulfonate, Photochem. Photobiol. Sci. 9 (2010) 323-330.
[5] V. Maurino, D. Borghesi, D. Vione, C. Minero, Transformation of phenolic compounds upon UVA irradiation of anthraquinone-2-sulfonate, Photochem. Photobiol. Sci. 7 (2008) 321-327.
[6] A. Bedini, E. De Laurentiis, B. Sur, V. Maurino, C. Minero, M. Brigante, G. Mailhot, D. Vione, Phototransformation of anthraquinone-2-sulphonate in aqueous solution, Photochem. Photobiol. Sci. 11 (2012) 1445-1453.

concentration was also at least five-fold lower, one can conclude that NB would absorb radiation at least 25 times less compared to AQ2S. Therefore, when calculating the photon flux absorbed by AQ2S, one is fully justified to assume that AQ2S is the only light-absorbing species in solution under the used UVA lamp. The photon flux absorbed by AQ2S can thus be expressed as $P_a^{AQ2S} = \int_\lambda \left[p^o(\lambda) \cdot (1 - 10^{-(A_{AQ2S}(\lambda))} \right] d\lambda$, where $p^o(\lambda)$ is the incident spectral photon flux density of the lamp and $A_{AQ2S}(\lambda)$ is the absorbance of AQ2S in the irradiated system. In particular, with [AQ2S] = 0.1 mM under the used array of UVA lamps, one gets $P_a^{AQ2S} = 2.0 \cdot 10^{-6}$ Einstein L^{-1} s^{-1}.

The linear trend of R_{NB} *vs.* NB concentration, shown in **Figure SM2**, is consistent with **equation (S2)**. In particular, from the experimental data one gets $R_{NB} = (7.96 \pm 0.35) \cdot 10^{-6}$ [NB] (with R_{NB} in M s^{-1} and [NB] in molarity) and, upon comparison with **equation (S2)**, one derives $\Phi_{^3AQ2S^*} \cdot P_a^{AQ2S} \cdot k_{^3AQ2S^*,NB} \cdot (k_{^3AQ2S^*})^{-1} = (7.96 \pm 0.35) \cdot 10^{-6}$. From the known values of $\Phi_{^3AQ2S^*}$ (0.18), $k_{^3AQ2S^*}$ (5.0·10^6 s^{-1}) and P_a^{AQ2S} (2.0·10^{-6} Einstein L^{-1} s^{-1}), one gets $k_{^3AQ2S^*,NB} = (1.1 \pm 0.1) \cdot 10^8$ M^{-1} s^{-1}. This result is in excellent agreement with a previous rate constant value obtained by using the laser flash photolysis technique and following the quenching of ^{3}AQ2S*.[4] Therefore, it is suggested that the quenching of ^{3}AQ2S* by NB can be fully accounted for by chemical reactivity, while physical quenching phenomena can be excluded.
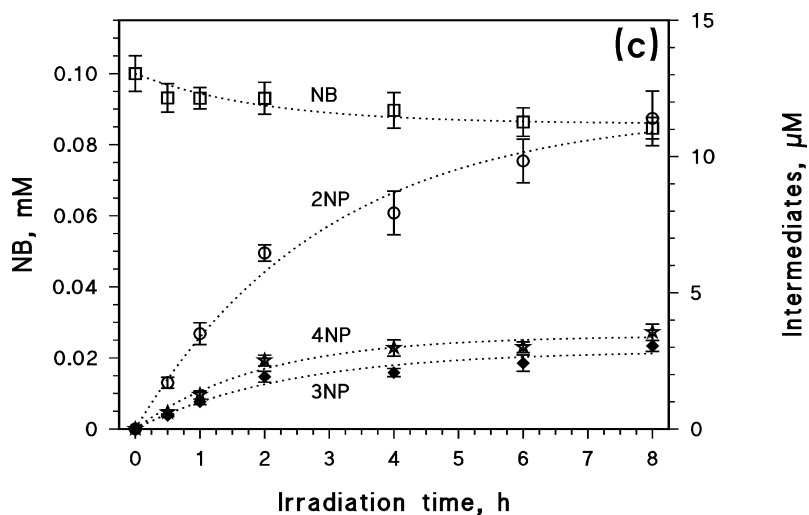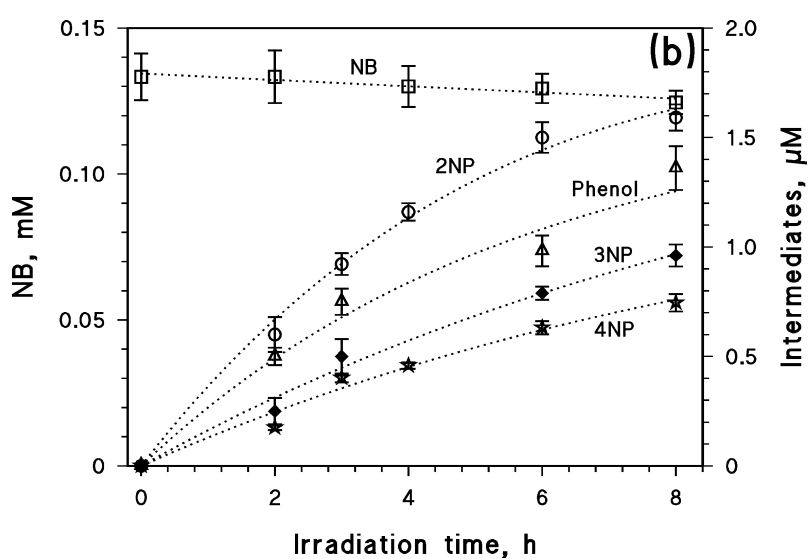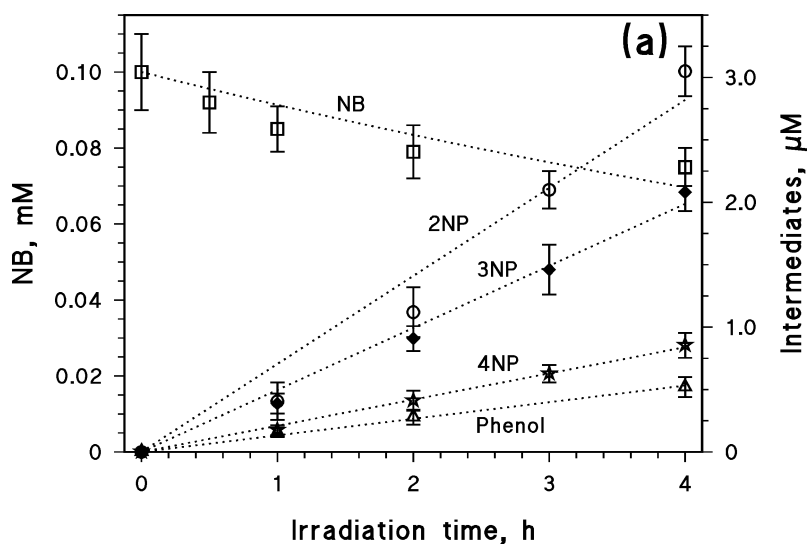
Figure SM3. Time evolution of 0.13 mM NB and of its transformation intermediates (phenol, 2NP, 3NP, 4NP) obtained by direct photolysis (SM3a), irradiation with H_2O_2 (SM3b), and irradiation with AQ2S (SM3c). The reported concentration values are the average of three replicas, error bars represent $\pm\sigma$.

COMPUTATIONAL SET-UP AND METHODOLOGY

Quantum mechanical modeling techniques were employed to determine the reaction mechanism and to evaluate the formation of phenol in the reactions of NB with $^\bullet$OH.

Computational Models

The molecular models were created by using the mean bond distances, the geometric parameters of the benzene ring, tetrahedral angles for sp^3-hybridized carbon and oxygen atoms, and 120° for sp^2-hybridized carbon atoms. In the calculation of the hydroxylated radicals, the aromatic ring was left planar except for the position of attack, and the attacking $^\bullet$OH was assumed to form a tetrahedral angle with the C-H bond due to the change in the hybridization state of the carbon atom from sp^2 to sp^3.

Methodology

Geometry optimizations of the reactants, the product radicals, pre-reactive and the transition state complexes were performed with the DFT method within the GAUSSIAN 03 package. The reaction system under consideration consists of $^\bullet$OH radicals, in other words open-shell species. It is well-known that open-shell molecules pose severe problems in quantum mechanical calculations. However, DFT methods use the exact electron density instead of molecular orbitals to calculate molecular properties and energies, thus they take electron correlation into account. They do not suffer from spin contamination, and this feature makes them suitable for calculations involving open-shell systems. The DFT calculations were carried out using the hybrid B3LYP functional, which combines HF and Becke exchange terms with the Lee-Yang-Parr correlation functional.

The choice of the basis set is very important in quantum mechanical calculations for reactions involving open-shell species. In previous studies, B3LYP/6-311+G(d,p)//B3LYP/6-31G(d) has been found to be the most suitable level of theory to predict energy barriers of radical addition reactions.[7,8] Based on these results, optimizations in the present study were performed at the B3LYP/6-31G(d) level followed by single point energy calculations at the B3LYP/6-311+G(d,p) level. The forming C-O bonds in the reaction paths were chosen as the reaction coordinates in the

---

[7] M. W. Wong. L. Radom. Radical additions to alkenes: Further assessment of theoretical procedures, J. Phys. Chem. A 102 (1998) 2237-2245.

[8] A. S. Ozen, V. Aviyente, R. A. Klein, Modeling the oxidative degradation of azo dyes: A density functional theory study. J. Phys. Chem. A. 107 (2003) 4898-4907.

determination of the transition states. Ground-state and transition-state structures were confirmed by frequency analyses at the same level. Transition structures were characterized by having one imaginary frequency that belonged to the reaction coordinate, corresponding to a first-order saddle point. Zero-point vibrational energies (ZPEs) were calculated at the B3LYP/6-31G(d) level. The same ZPEs were used for the B3LYP/6-311+G(d,p)//B3LYP/6-31G(d) calculations. IRC calculations were performed for all of the transition geometries, and the corresponding maxima were confirmed.

Solvent Effect Model

Solvation plays a decisive role in determining the energetics of the degradation reactions of organic compounds in aqueous media. The solvation process in such reactions has been approached theoretically by several methods. Polarizable continuum methods (PCMs) represent a formally simple and popular approach to solvation due to their flexibility and efficiency.[9] In PCMs, the solute molecule is placed in a cavity surrounded by a polarizable continuum, whose reaction field modifies the energy and the properties of the solute. The geometry of the cavity is determined by the shape of the solute. The reaction field is described in terms of apparent polarization charges or reaction field factors included in the solute Hamiltonian, so that it is possible to perform iterative procedures leading to the self – consistence between the solute wave-function and the solvent polarization.

On the other hand, water molecules induce geometry relaxation on the solute molecules. This effect becomes more important when hydrogen-bonded complexes are present, which is the case of the reactions investigated here. However, the results obtained in earlier studies indicate that geometry changes have a negligible effect on the energy of the solute in water for both open and closed shell structures.[10] Therefore, in this study, in order to take into account the effect of solvent H_2O on the energetics and the kinetics of the NB + $^\bullet$OH reactions, DFT/B3LYP/6-311+G(d,p) calculations were carried out for the optimized structures of the reactants, the pre-reactive and the transition state complexes and the product radicals, by using COSMO (conductor-like screening solvation model)[10] as the solvation model, implemented in the GAUSSIAN 03 package. The solvent was water at 25° C, with dielectric constant $\varepsilon = 78.39$. COSMO is one of the PCMs and it describes the solvent reaction field by means of apparent polarization charges distributed on the

[9] N. S. Hush, J. Schamberger, G. B. Bacskay. A quantum chemical computational study of the relative stabilities of cis- and transplatinum dichloride in aqueous solution. Coord. Chem. Rev. 249 (2005) 299-311.

[10] V. Barone, M. Cossi, Quantum calculation of molecular energies and energy gradients in solution by a conductor solvent model. J. Phys. Chem. A. 102 (1998) 1995-2001.

cavity surface, which are determined by imposing that the total electrostatic potential cancels out on the surface. This condition can describe the solvation in polar liquids. Hence, it is the method of choice in this study.

Reactants and Product Radicals

Four different radicals were determined as the products of the reaction between nitrobenzene and the $^\bullet$OH radical. The electronic and thermodynamic properties of the most stable conformers were also calculated. Figure 1 in the manuscript represents the potential energy profile of the DFT-modeled mechanism for the initial attack of the $^\bullet$OH radical to nitrobenzene.

The total energies for each of the radicals obtained for both gas and aqueous media indicate that all the radicals have hydrogen-bond-like stabilizations. The interaction distance between the original hydrogen atom at the addition center and the oxygen atom of the added •OH was calculated to be 1.997 $^\circ$A for *p*-R, 2.073 $^\circ$A for *m*-R, and 2.001 A for *o*-R. For the gas phase, among the four radicals produced, *p*-R has the lowest energy and is, therefore, the most stable one while *m*-R is the least stable radical. The *m*-R is around 5.44, *o*-R around 2.04 and *i*-R is around 4.05 kcal mol^{-1} less stable than *p*-R. For the aqueous phase, the sequence remains the same. The most and the least stable radicals are again the *p*-R and the *m*-R, respectively. However, all the product radicals are more stable in the aqueous phase, due to the newly formed hydrogen-bonds between their H atoms and the O atoms of the water molecules. The stabilities of the radicals increase by around 15.3 kcal mol^{-1} in the aqueous solution. Adopting the localization approach of the Wheland's approximation, it may be predicted that para-addition is the most probable reaction path for both gas and aqueous phases. The products of the four addition paths lie ca. 15 kcal mol^{-1} below the reactants. It may be concluded that the reactions will proceed to the corresponding products, once the reactants are sufficiently close to each other. The thermodynamically most favored product is 1-hydroxy-2-nitrocyclohexadienyl radical, followed by 1-hydroxy-4-nitrocyclohexadienyl radical for both gas and aqueous phases.
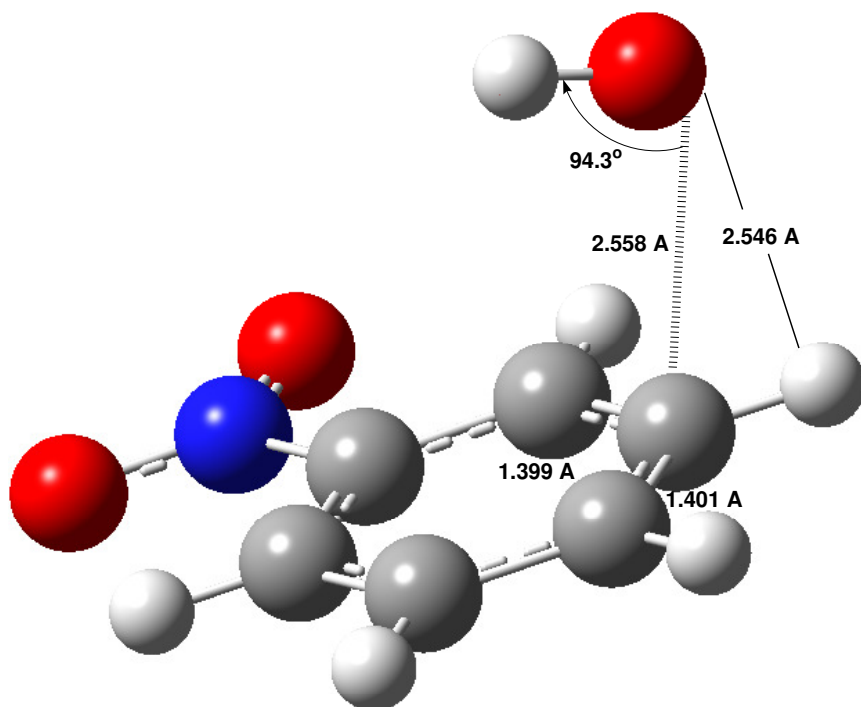
Pre-reactive complexes

Our calculations indicated the formation of weakly-bound complexes between the $^\bullet$OH radical and nitrobenzene as the precursors of the reactions. Due to the existence of these pre-reactive van der Waals complexes, the reaction paths under investigation proceed over barriers that are lower in energy than the reactants. The pre-reactive complexes exert strong influence over the kinetics of the

reactions by altering barrier heights and affecting the energy partitioning of the reaction products. Furthermore, the presence of such complexes affects the reaction dynamics by spatially directing the site of the reaction, either by steric direction or by providing a low potential well that favors a reaction site.

Depending on the direction of approach of the $^\bullet$OH radicals, four different chemically activated pre-reactive complexes, o-PC, m-PC, p-PC and i-PC with shallow wells, ca. 6.00 and 1.25 kcal mol^{-1} were determined for gas and aqueous phases respectively. The optimized structures of the pre-reactive complexes are shown in **Figure SM4**. The $^\bullet$OH radical is seen to approach the aromatic ring from above, lying almost parallel to the ring plane with a deviation of about 0.5-1.0$^{\text{o}}$. The hydrogen atom was found to be facing towards the center of the ring, while the ring carbons at the addition centers were found to deviate from the ring plane by around 2$^{\text{o}}$. The main difference in the optimized geometries occurs in the distance between the oxygen atom of $^\bullet$OH and the ring carbon. o-PC has the longest distance among all the complexes. Energetically the p-PC, m-PC and o-PC are the most stable complexes, lying 2.38, 2.32 and 2.31 kcal mol^{-1} below the isolated reactants, respectively. In aqueous media, the least stable pre-reactive complex is the i-PC, which is around 1.52 kcal mol^{-1} less stable than p-PC. It was observed that the stability of the pre-reactive complexes is higher in the aqueous than in the gas phase. The presence of water molecules, hydrogen-bonded to the hydrogen atoms of the complexes, was found to lower the total energies. The reduction in energy was calculated to be ca. 14.63 kcal mol^{-1}.
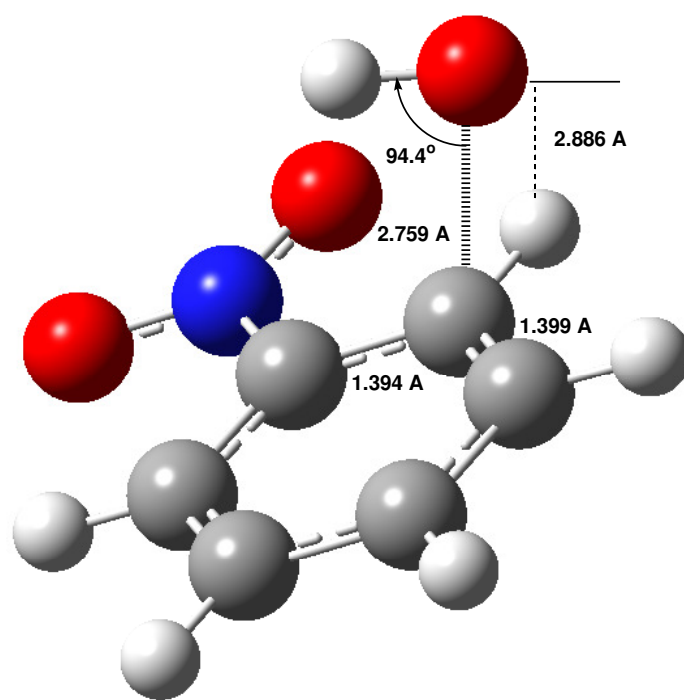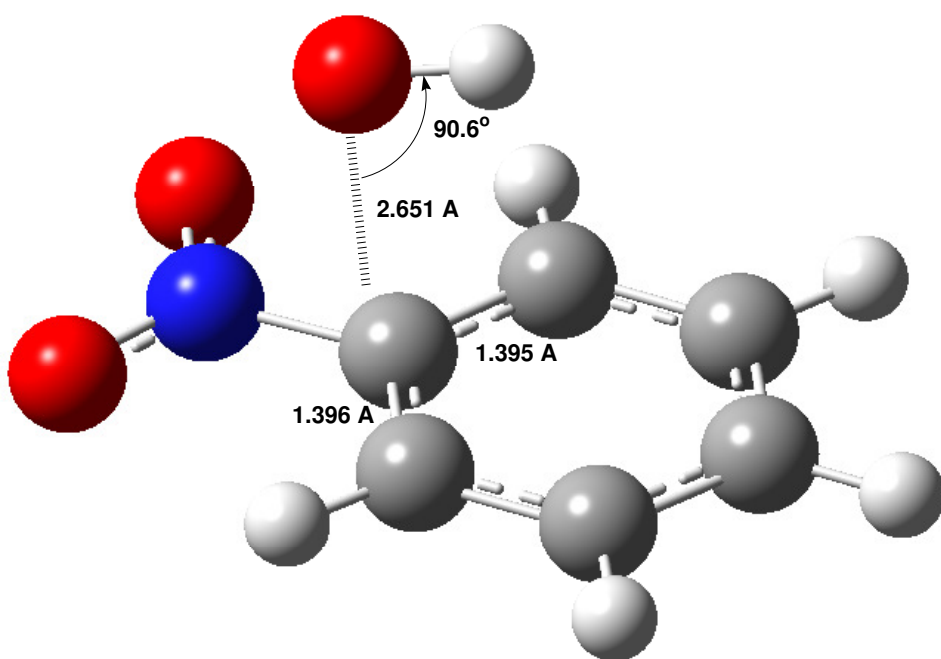
o-PC

m-PC
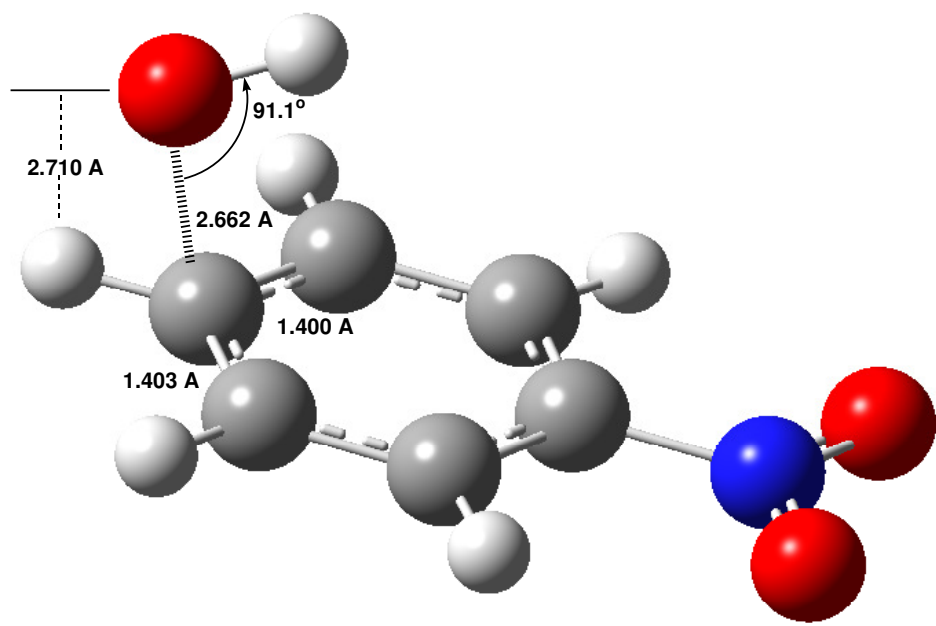
p-PC

i-PC

Figure SM4. The optimized structures of the pre-reactive complexes.

Transition state complexes

Four transition state complexes *o*-TS, *m*-TS, *p*-TS and *i*-TS, one for each of the possible reaction paths were identified. The optimized structures of the TS are displayed in **Figure SM5**. In all the complexes the •OH radical is oriented such that it is almost parallel to the ring plane. The oxygen atom points to the carbon atom at the reaction center, while the hydrogen atom points to the center of the aromatic ring. The major structural changes in the ring geometry relative to the parent nitrobenzene molecule are all localized around the carbon atom at the reaction center. The two C-C bonds connecting the addition center lengthen, while the lengths of the subsequent bonds remain the same. This finding indicates that the two C-C bonds connecting the addition center have single rather than double bond character. The ones away from the addition center have a more pronounced double bond character.

In the light of the potential energy profiles, it may be suggested that the forming bond length is a sensitive measure of the formation of the transition state complex along the reaction coordinate. As displayed in **Figure SM5**, *p*-TS and *i*-TS have much longer C-O bonds, 2.511 Å and 2.622 Å respectively, as compared to the C-O bonds in *m*-TS and *o*-TS. This suggests that *p*-TS and *i*-TS are early transition states, whereas *m*-TS and *o*-TS are formed late along the reaction coordinate. Among the four complexes the longest C-O bond belongs to the *i*-TS followed by *p*-TS, while the *m*-TS and *o*-TS have much shorter C-O bonds. This indicates that they are formed late as compared to *i*-TS and that, therefore, *i*-TS is the earliest transition state. Furthermore, the *i*-TS and *p*-TS were found to have the lowest total energies among all the possible transition states, indicating that they are thermodynamically stable. All the transition state structures, *i*-TS, *p*-TS, *o*-TS and *m*-TS lie 0.76, 2.33, 0.66 and 0.31 kcal mol^{-1}, respectively, below the reactants. Thus, it may be concluded that in the photo-oxidative degradation of nitrobenzene, *i*-TS and *p*-TS occur early along the reaction coordinate, giving rise to long C-O bonds and low total energies. Although the energies of all the transition state complexes decrease by around 15 kcal mol^{-1}, the *p*-TS and *i*-TS are the most thermodynamically stable TS structures for the aqueous phase as well.
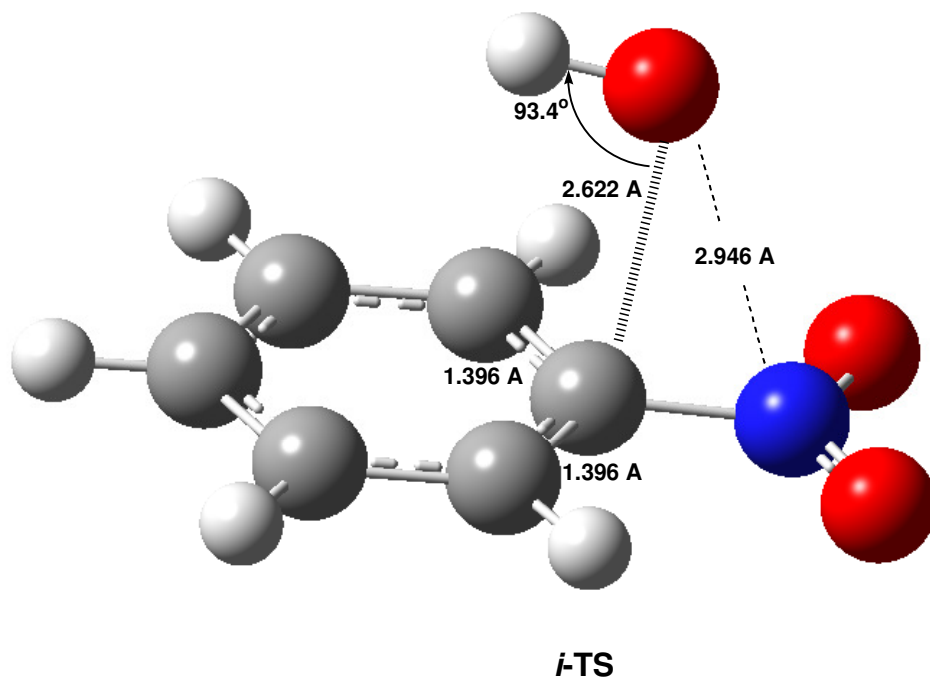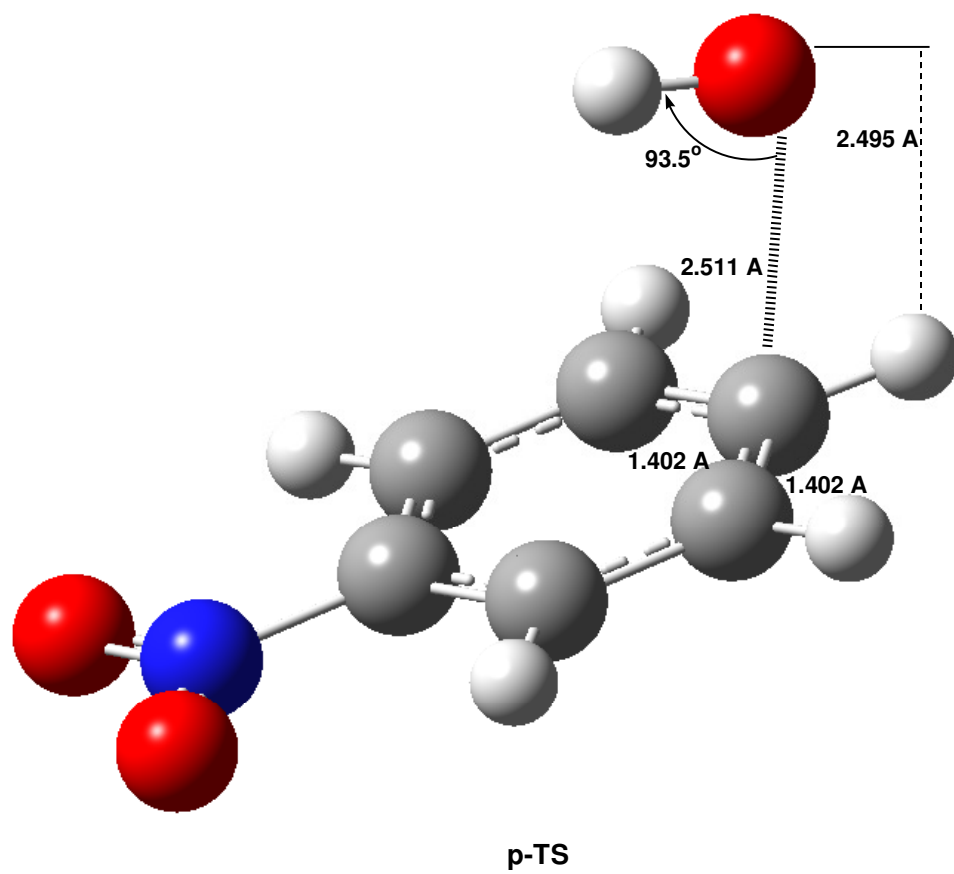
o-TS

m-TS

p-TS

_i_-TS
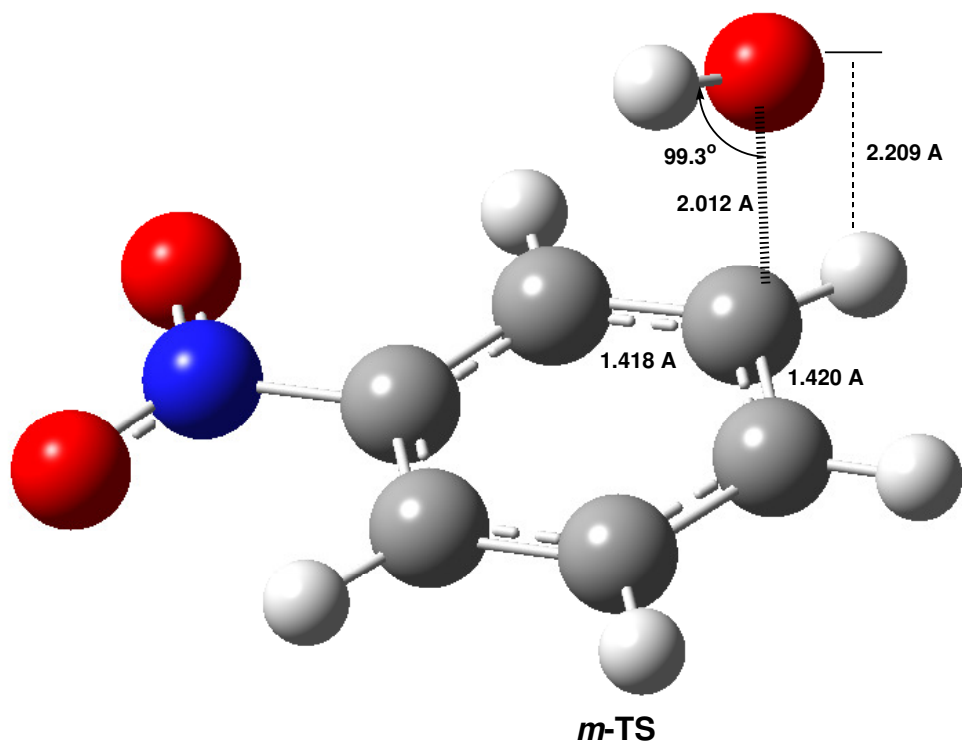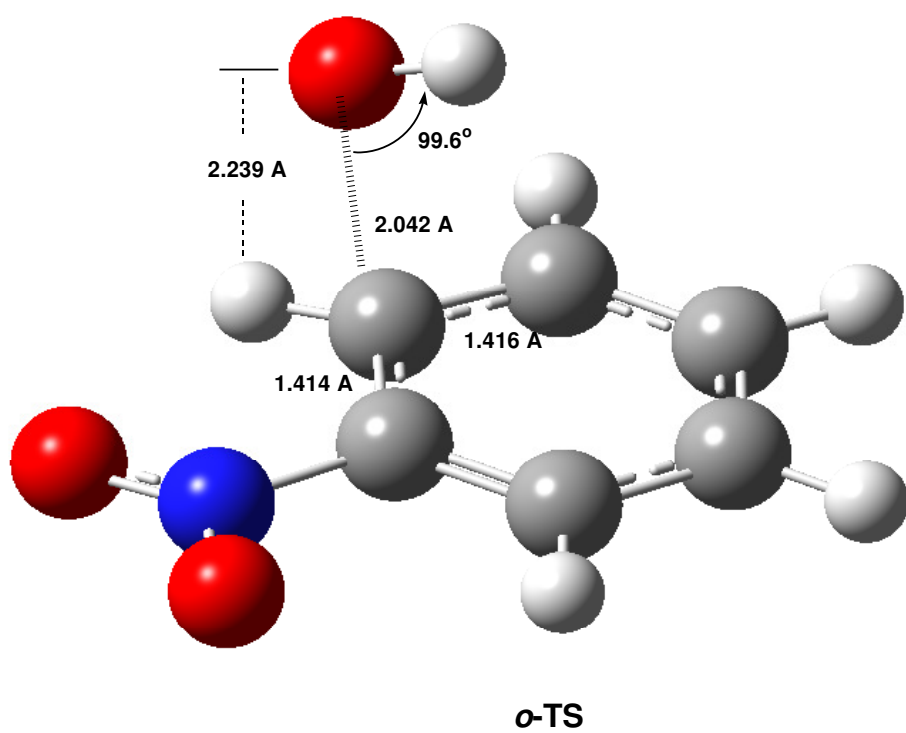
Figure SM5. The optimized structures of the transition state complexes.

Energetics of the reaction paths

The activation energies E_a for the four possible reaction paths were calculated and presented in **Table SM1** along with the reaction energies ΔE_r for both gas and aqueous phases. The values in **Table SM1** show that the lowest activation energy belongs to the *para*-addition path. The energy barrier for the *ipso*-addition path is 0.048 kcal mol^{-1} higher than the energy barrier for the *para*-addition path. In the aqueous phase, the stability order of the transition state complexes remains the same. Although solvent water has a stabilizing effect in terms of total energies, the energy barriers in aqueous solution for *para*- and *ipso*-addition paths are slightly higher than the barriers in gas phase. They increase by around 0.041 and 0.033 kcal mol^{-1} respectively, because of the prevention of the formation of the nice intramolecular hydrogen-bond network observed in the two transition state complexes. In contrast, the activation energies for the *ortho*- and *meta*-addition paths decrease by 0.649 and 0.206 kcal mol^{-1}. The reason may be attributed to the additional stabilizing effect of the newly formed hydrogen-bonds with the water molecules. Moreover, *para*-addition path was found to have the highest exothermicity in both gas and aqueous phases. The result is consistent with Hammond's postulate, which states that early transition states have low energy barriers and high exothermicities. So, it may be concluded that *p*-TS and *i*-TS are the most probable transition states for gas and aqueous phases, respectively.

Table SM1. Activation energies E_a, reaction energies E_r, rate constants k and product distributions for the possible reaction paths.

	o-Addition	*m*-Addition	*p*-Addition	*i*-Addition
Gas phase				
$E_a(kcal\ mol^{-1})$	2.006	1.658	0.0503	0.0978
$E_r(kcal\ mol^{-1})$	-16.169	-12.768	-18.205	-14.152
$k(cm^3 molecule^{-1}s^{-1})$	0.16×10^6	0.29×10^6	11.99×10^6	19.78×10^6
Branching ratio(%)	0.98	1.78	36.70	60.55
Aqueous phase				
$E_a(kcal\ mol^{-1})$	1.357	1.452	0.0913	0.131
$E_r(kcal\ mol^{-1})$	-16.801	-11.846	-17.733	-12.315
$k(cm^3 molecule^{-1}s^{-1})$	0.49×10^6	0.40×10^6	11.20×10^6	18.70×10^6
Branching ratio(%)	3.09	2.53	35.35	59.03

Reaction rates and product distribution

The rate constant *k* for each reaction path was calculated by using the Transition State Theory for 300 K. The classical rate constant k in the Transition State Theory is given by **Eq. (S3)**:

$$k = \frac{k_B T}{h} \frac{q_{TS}}{q_T . q_{OH}} e^{-Ea/RT} \tag{S3}$$

where k_B is Boltzmann's constant, *T* is temperature, *h* is Planck's constant, *q*'s are molecular partition functions for TS and the reactant species, nitrobenzene and $^\bullet$OH, and E_a is the activation energy. Each of the molecular partition functions was assumed to be the product of translational, rotational, vibrational and electronic partition functions of the corresponding species.

The calculated rate constants in **Table SM1** show that the highest rate constant belongs to *ipso*-addition, followed by *para*-addition, whereas *ortho*- and *meta*- addition paths are much slower consistent with their high energy barriers. The branching ratio for each of the reaction paths was calculated by dividing the corresponding rate constant by the sum of the rate constants, taking the number of similar addition centers into account. By using the branching ratios, the relative concentrations of the primary intermediates were also calculated and they are presented in **Table SM1.** The results indicate that *ipso*-addition is the dominant reaction path for both gas and aqueous phases, followed by *para*-addition. Moreover, the calculated rate constants show that *meta*- and *ortho*-addition proceed faster in the aqueous phase compared to the gas phase. In contrast, the rates of the remaining paths decrease slightly in aqueous solution, coherently with the increase in the energy barriers due to the weakening effect of water molecules on the original hydrogen bonds in the pre-reactive complexes.

The product distribution obtained indicates that the major primary intermediate formed in the photo-oxidative degradation of nitrobenzene is the *i*-R (1-hydroxy-1-nitrocyclohexadienyl radical) which then forms phenol through abstraction of the nitro group. The reaction also yields *p*-R (1-hydroxy-4-nitrocyclohexadienyl radical) which then forms 4-nitrophenol through the abstraction of the redundant ring hydrogen by molecular oxygen. The relative concentrations of *o*-R and *m*-R which are then converted to 2-nitrophenol and 3-nitrophenol through the reaction with O_2 are lower than all the other reaction products. The computational results indicate that the products of the photo-oxidative degradation of nitrobenzene are phenol (P), 4-nitrophenol (4NP), 2-nitrophenol (2NP) and 3-nitrophenol (3NP), with [P] > [4NP] > [3NP] > [2NP] in the gas phase. The concentration order is [P] > [4NP] > [2NP] > [3NP] in the aqueous phase.
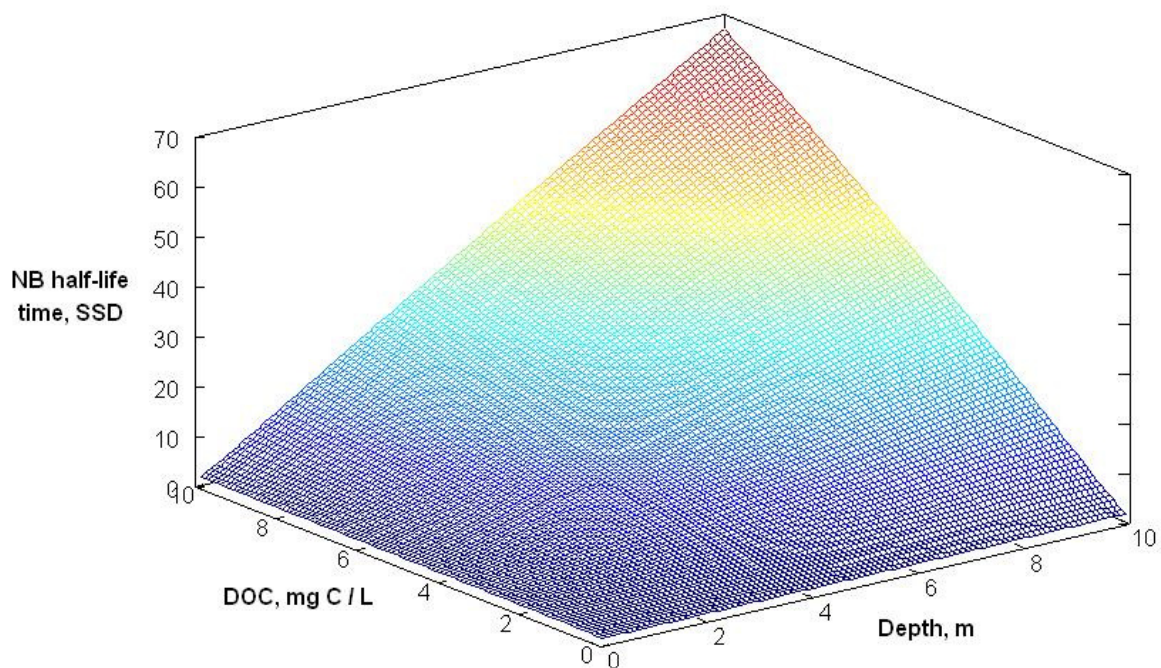
Figure SM6. Modelled half-life time of NB as a function of depth and DOC. Other water conditions: 0.1 mM nitrate, 1 µM nitrite, 1 mM bicarbonate, 10 µM carbonate. SSD = summer sunny day, equivalent to fair-weather 15 July at 45° N latitude.